Modal Analysis of Fluid Flows: Applications and Outlook

Kunihiko Taira*
University of California, Los Angeles, California 90095
Maziar S. Hemati†
University of Minnesota, Minneapolis, Minnesota 55455
Steven L. Brunton‡
University of Washington, Seattle, Washington 98195
Yiyang Sun§
University of Minnesota, Minneapolis, Minnesota 55455
Karthik Duraisamy¶
University of Michigan, Ann Arbor, Michigan 48109
Shervin Bagheri**
Royal Institute of Technology (KTH), Stockholm 10444, Sweden
Scott T. M. Dawson††
Illinois Institute of Technology, Chicago, Illinois 60616
and
Chi-An Yeh‡‡
University of California, Los Angeles, California 90095

DOI: 10.2514/1.J058462

Kunihiko Taira is an Associate Professor of Mechanical and Aerospace Engineering at the University of California, Los Angeles. Prior to his current position, he was an Associate Professor at the Florida State University. He received his B.S. from the University of Tennessee, Knoxville, and his M.S. and Ph.D. from the California Institute of Technology. He is a recipient of the 2013 U.S. Air Force Office of Scientific Research and 2016 U.S. Office of Naval Research Young Investigator Awards. He is an Associate Fellow of the AIAA.

Maziar S. Hemati is an Assistant Professor of Aerospace Engineering and Mechanics at the University of Minnesota Twin Cities. He earned his B.S. in Aerospace Engineering, and his M.S. and Ph.D. in Mechanical Engineering all from the University of California, Los Angeles. He is the recipient of the 2019 U.S. Air Force Office of Scientific Research Young Investigator Award. He is a Senior Member of the AIAA.

Steven Brunton is an Associate Professor of Mechanical Engineering at the University of Washington. He received his B.S. in Mathematics from the California Institute of Technology in 2006, and his Ph.D. in Mechanical and Aerospace Engineering from Princeton University in 2012. He received the U.S. Army and U.S. Air Force Young Investigator Awards, the Presidential Early Career Award for Scientists and Engineers, and the SIAM Activity Group on Computational Science and Engineering Early Career Prize. He is a Member of the AIAA.

Received 13 March 2019; revision received 26 July 2019; accepted for publication 5 August 2019; published online Open Access 11 October 2019.

*Associate Professor, Mechanical and Aerospace Engineering. Associate Fellow AIAA.
†Assistant Professor, Aerospace Engineering and Mechanics. Senior Member AIAA.
‡Associate Professor, Mechanical Engineering. Member AIAA.
§Postdoctoral Associate, Aerospace Engineering and Mechanics. Member AIAA.
¶Associate Professor, Aerospace Engineering. Member AIAA.
**Associate Professor, Mechanics.
††Assistant Professor, Mechanical, Materials, and Aerospace Engineering. Member AIAA.
‡‡Postdoctoral Research Scholar, Mechanical and Aerospace Engineering. Member AIAA.

I. Introduction

THE field of fluid mechanics involves a range of rich and vibrant problems with complex dynamics stemming from instabilities, nonlinearities, and turbulence. The analysis of these flows benefits from having access to high-resolution spatiotemporal data that capture the intricate physics. With the rapid advancement in computational hardware and experimental measurement techniques over the past few decades, studies of ever more complex fluid flows have become possible. Although these analyses provide great details of complex unsteady fluid flows, we are now faced with the challenge of analyzing vast and growing data and high-dimensional nonlinear dynamics representing increasingly complex flows.

Although the analysis of these complex flows may appear daunting, the fact that common flow features emerge across a wide spectrum of fluid flows or over a large range of nondimensional flow parameters suggests that there are key underlying phenomena that serve as the foundation of many flows. The emergence of these prominent features, including the von Kármán vortex shedding and the Kelvin–Helmholtz instability, provides hope that a lot of the flows we encounter share low-dimensional features embedded in high-dimensional dynamics. Shown, as an example, in Fig. 1 is a photograph taken from the Space Shuttle STS-100 of the von Kármán vortex street generated by the Rishiri Island in Japan, whose wake is visualized by the clouds.[§§] Let us compare this image with the two-dimensional (2-D) low-Reynolds-number flow over a circular cylinder shown in the same figure. The striking similarity between these two flows suggests the existence of spatial features that capture the essence of the flow physics. In this work, we present modal-analysis techniques to mathematically extract the underlying flow features from flowfield data or the flow evolution operators.

In addition to flow analysis, modal-decomposition techniques can also be used to facilitate reduced-order flow modeling and control. Indeed, modal-decomposition techniques offer a powerful means of identifying an effective low-dimensional coordinate system for capturing dominant flow mechanisms. The reduction of the system order corresponds to the choice of an appropriate (reduced basis) coordinate system to represent the fluid flow. This concept has implications for nearly every ensuing modeling and control decision. A

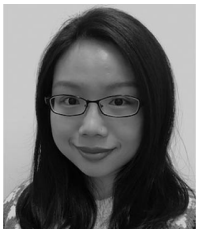

Yiyang Sun is a Postdoctoral Associate of Aerospace Engineering and Mechanics at the University of Minnesota Twin Cities. She received her B.S. in Naval Architecture and Ocean Engineering from the Huazhong University of Science and Technology, and her Ph.D. in Mechanical Engineering from the Florida State University. She is a Member of the AIAA.

Karthik Duraisamy is an Associate Professor of Aerospace Engineering at the University of Michigan. He received his M.S. and Ph.D. from the University of Maryland. At the University of Michigan, he is the Director of the Center for Data-Driven Computational Physics and the U.S. Air Force Center of Excellence on Rocket Combustor Dynamics. He is a Member of the AIAA.

Shervin Bagheri is an Associate Professor in the Department of Mechanics at the Royal Institute of Technology (KTH) in Stockholm. His research focuses on active and passive control of fluid flows. He is a Wallenberg Academy Fellow and one of the 20 recipients of the Future Research Leaders grants awarded every three years by the Swedish Foundation for Strategic Research.

Scott Dawson is an Assistant Professor in the Mechanical, Materials and Aerospace Engineering Department at the Illinois Institute of Technology. Prior to this, he was a postdoctoral scholar within the Graduate Aerospace Laboratories at the California Institute of Technology. He completed his undergraduate studies at Monash University, and his Ph.D. in Mechanical and Aerospace Engineering at Princeton University. He is a Member of the AIAA.

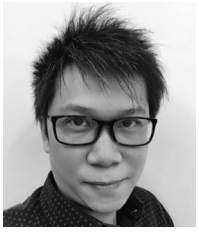

Chi-An Yeh is a Postdoctoral Scholar of Mechanical and Aerospace Engineering at the University of California, Los Angeles. He received his B.S. from the National Chiao Tung University, M.S. from the National Taiwan University, and Ph.D. from the Florida State University, all in Mechanical Engineering. He is a Member of the AIAA.

[§§]STS-100 Shuttle Mission Imagery, NASA, https://spaceflight.nasa.gov/gallery/images/shuttle/sts-100/html/sts100-710-182.html [accessed March 2019].

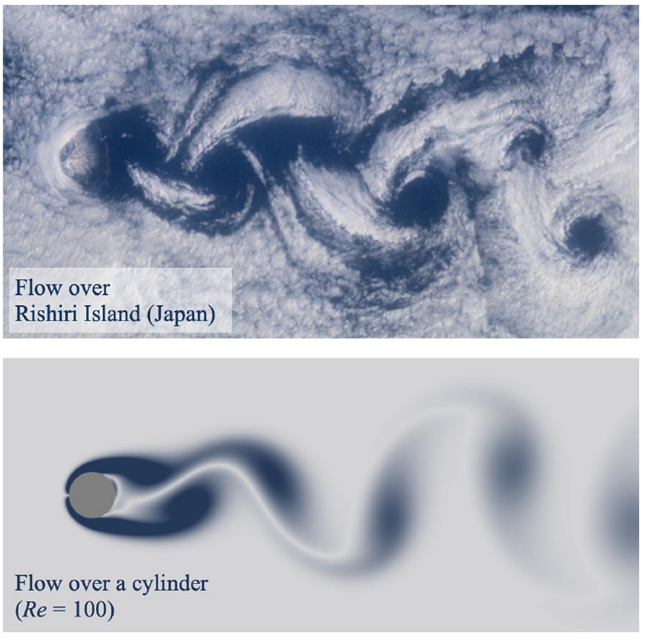

Fig. 1 Von Kármán vortex street generated by the Rishiri Island in Hokkaido, Japan (top: photograph from NASA, 2001; STS-100); this wake produced at a high Reynolds number shares great similarity with the cylinder wake at a low Reynolds number (bottom).

linear subspace to describe the flow, for example, obtained via proper orthogonal decomposition (POD), is the most common choice for a low-dimensional basis. After the choice of a coordinate system, there are two main distinctions in modeling procedures: depending on 1) whether or not the model is physics based or data driven, and 2) whether or not the model is linear or nonlinear. Further discussion of approaches for modeling and controlling fluid flows will be explored throughout the paper, with particular emphasis in the Outlook section.

The present paper is one of the products from the AIAA Discussion Group on Modal Decomposition Methods for Aerodynamic Flows (2015–2018) organized under the support of the AIAA Fluid Dynamics Technical Committee. The goal of this discussion group was to provide an educational service to nonspecialists who seek to gain greater insights from fluid flows with modal-decomposition and modal-analysis methods. Since the discussion group started in 2015, invited sessions were organized at the 2016, 2017, and 2018 AIAA Aviation meetings. The insights gained from various discussion group activities led to the previous overview paper on modal-analysis methods that focused on a broad review at a fundamental level [1]. The modal-analysis methods described at length in the previous overview paper make up an arsenal of versatile tools relevant for extracting concise and interpretable characterizations of complex spatiotemporal flowfield data, or the operators that generated them. In the first overview paper, we covered the POD [2,3], balanced POD (BPOD) [4,5], dynamic mode decomposition (DMD) [6–9], Koopman analysis [7,10], global stability analysis [11,12], and resolvent analysis [13,14].

The first overview paper [1] focused on the how-to aspects of modal-analysis methods, whereas the present effort aimed to demonstrate how the outputs of these modal-analysis techniques can be interpreted to elucidate physical insights. Indeed, a blind application of a modal-analysis method is rarely a worthwhile endeavor. The compilation of the present paper is primarily motivated by the fact that the true power of modal-analysis techniques in practice stems from the user's ability to appropriately apply these methods and to interpret the associated outputs. In addition to this second overview paper, we have assembled a number of modal-analysis papers to form a special section in the *AIAA Journal* to document the efforts of the discussion group. The purpose of this special section of the present issue is to serve as an educational support to provide sufficient guidance on how modal-analysis techniques can be used to extract useful and relevant information from otherwise complex flow physics. We assume here that readers of this paper are familiar with the basics of modal-decomposition and modal-analysis techniques covered in the first overview paper [1]. For this reason, we do not reintroduce the algorithms for performing modal analysis, but rather focus on presenting the interpretations of the results from these analyses.

In what follows, we select a few applications of modal-analysis techniques on a number of canonical flows that capture fundamental flow features in many engineering and scientific settings. In particular, we consider examples of cylinder wakes, wall-bounded flows, airfoil wakes, and cavity flows. A short summary of the topics covered in this paper is compiled in Table 1. The examples within this overview paper are mostly of a computational nature. However, this should not discourage users from employing relevant modal-analysis techniques to analyze experimental fluid flows. Experimental data sets introduce a unique set of challenges (e.g., noisy and band-limited data) that must be considered carefully when using data-driven analysis methods. In this overview, we highlight some of the prevailing challenges for analyzing experimental data, and point to best practices and relevant references where applicable. We also note that the references highlighted in the following examples are not necessarily the first to perform a modal analysis of the associated flows. Recent citations are provided in the paper to serve as an educational guidance, and chosen in hopes of facilitating interested readers to dive further into past literature. Emphasis of the discussions is placed on how different modal-analysis techniques can complement one another to reveal different characteristics of the flow, build reduced-order models (ROMs), and provide guidance for flow control. Toward the latter part of the paper, we offer an outlook on modal analysis within fluid mechanics.

II. Cylinder Wakes

Flow over a circular cylinder is one of the most fundamental flows in fluid mechanics for its relevance in engineering settings and for capturing the essential features of bluff-body flows [15,16]. For these reasons, there have been a tremendous amount of analyses performed on various aspects of cylinder flows, including its wake [17–22], aerodynamic forces [23], stability [24–26], compressibility [27], fluid–structure interactions [28,29], and flow control [30–33]. Over the past two decades, modal-analysis techniques have played crucial roles in uncovering additional insights into the cylinder wake dynamics. Although we cannot provide a complete review of the modal analyses performed on cylinder flows, we discuss some modal-analysis studies that describe the wake dynamics and suppress unsteadiness with flow control using mode-based ROMs.

Over a wide range of Reynolds numbers, cylinder flows exhibit the distinct von Kármán shedding wake, even under the presence of spanwise instabilities and turbulence [15,16], as shown in Fig. 1. The fact that von Kármán shedding is identifiable from simple visual inspection suggests that such flow structures can represent the

Table 1 Outline of the present paper

	Sections	Keywords
I	Introduction	
II	Cylinder wakes	POD, DMD, global stability analysis, flow modeling, Galerkin projection, SINDy
III	Wall-bounded flows	POD, BPOD, DMD, global stability analysis, resolvent analysis, flow modeling, Galerkin projection, flow control
IV	Airfoil wakes	POD, DMD, global stability analysis, resolvent analysis, parabolized stability analysis, flow control
V	Cavity flows	POD, DMD, global stability analysis, resolvent analysis, flow control, aircraft application
VI	Outlook	Superposition, sparse and randomized algorithms, machine learning, ROMs, closure, hyper-reduction

flowfield in a low-dimensional manner. In other words, these flows can be compressed to these dominant flow features. It is worth mentioning that the cylinder wake provides an ideal setting for developing and testing modal-analysis techniques. Note that additional complexity in the flow is often desired to test modal-analysis techniques for many applications. Nonetheless, cylinder flow serves as an attractive initial test bed for development and for educational purposes. Beyond admitting low-dimensional dynamic representations, cylinder wakes have been widely studied and numerous investigations have been documented in the scientific and engineering literature. Furthermore, data from both physical experiments and numerical simulations are relatively simple to acquire and reproduce. The results of various modal-analysis techniques applied to cylinder wake are often among the easier results to interpret, and thus, provide a convenient entry point for developing intuition around these methods. For all these reasons, we begin by introducing various modal-analysis approaches within the context of the cylinder wake. The first portion of this discussion will be devoted to guiding the readers through the process of building intuition for each modal-analysis technique and for developing an appreciation for how to interpret the outputs of such analyses. The ensuing sections will focus on more advanced applications, highlighting recent efforts on uncovering flow physics associated with the cylinder wake.

A. Proper Orthogonal Decomposition

Let us first consider the data-based modal analysis of cylinder flow. Data-based techniques only need the flowfield data obtained from numerical simulations or experimental measurements, and do not require knowledge of the governing dynamics. In particular, we consider the POD, which can extract modal contents from a collection of snapshot data. The term *snapshot* is used in modal analysis to refer to flowfield data collected at an instance in time. Before performing POD of the snapshot data, each of the flowfield data at an instance in time needs to be formatted into a column vector. Details on formatting the snapshot to perform the POD analysis (as well as the DMD analysis) can be found in the appendix of the first overview paper [1]. Although we make exclusive use of the snapshot POD method in the present paper, analytical POD methods are also commonly employed for flow analysis and modeling.

If the velocity field is analyzed with POD, the modes $\boldsymbol{\varphi}_i(\boldsymbol{x})$ optimally capture the kinetic energy (KE) of the unsteady flowfield, and the eigenvalues λ_i represent the amount of KE held by each mode. That means that the POD analysis finds the best set of spatial modes to extract as much KE as possible in the flowfield over time. These POD modes are orthogonal to each other, ensuring the optimality of extracting KE by each individual mode. In a mathematically abstract sense, we can consider the POD analysis to be fitting a low-dimensional ellipsoid to the given data.

Let us demonstrate the use of POD on the 2-D unsteady laminar flow over a circular cylinder at a diameter-based Reynolds number of $Re = 100$. The cylinder flow analyzed here was obtained from direct numerical simulation (DNS) using the immersed boundary projection method [34,35]. An instantaneous snapshot of the cylinder flow is shown in Fig. 2 exhibiting von Kármán vortex shedding. For the POD analysis, we collect 325 snapshots of the flowfield over eight shedding periods. The data are compiled into a data matrix, upon which the snapshot POD [36] is applied. The snapshot-based method enables us to perform the decomposition in a computationally tractable manner when the dimension of an individual snapshot is much larger than the total number of snapshots [2,36]. In performing the POD here, we first subtract the mean from all snapshots, so that we can focus on modal structures associated with fluctuations. The extracted spatial POD modes $\boldsymbol{\varphi}_i(\boldsymbol{x})$ capture regions where fluctuations appear in the flow. Because this cylinder-flow example is a periodic flow, these spatial modes appear in pairs. This also suggests that the modes are based on advective physics with oscillator-type dynamics.

The POD analysis reveals that the fluctuations in the flowfield can be captured well with only a small number of mode pairs, as illustrated in Fig. 2. The first two, four, and six modes capture 94.84, 98.68, and 99.85%, respectively, of the flow fluctuations in terms of the KE. With eight modes, this percentage reaches 99.97%, which is essentially 100%. This means that the high-dimensional flowfield can be accurately expressed with only six or eight spatial modes, suggesting the possibility for significant compression of the flowfield data. That is, we reduce the representation of the flowfield from the number of grid points (times the number of flow variables) to merely the number of POD modes. The mode shapes associated with the dominant POD modes reveal the dominant energetic spatial structures in the flow. Interestingly, both POD modes 1 and 2 possess a top-down asymmetry, indicating that the dominant energetic structures are associated with the asymmetry of the von Kármán wake. As it will be discussed in a latter section, these POD modes can serve as a basis to construct an ROM that describes the dynamics of the flow. One of the important properties of the POD modes is the orthogonality of the modes (i.e., $\langle \boldsymbol{\varphi}_i, \boldsymbol{\varphi}_j \rangle = \delta_{ij}$), which is attractive for developing sparse reduced-order representation of the flow dynamics.

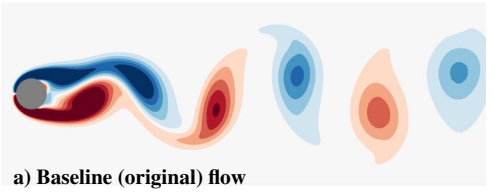

a) Baseline (original) flow

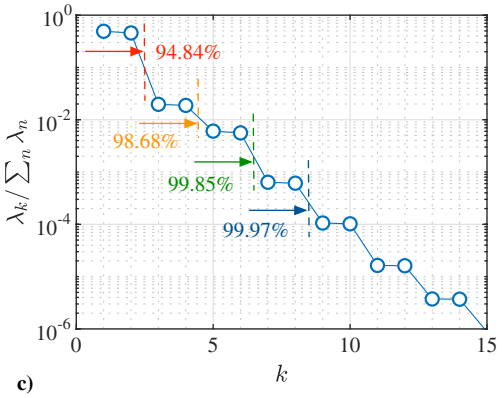

c)

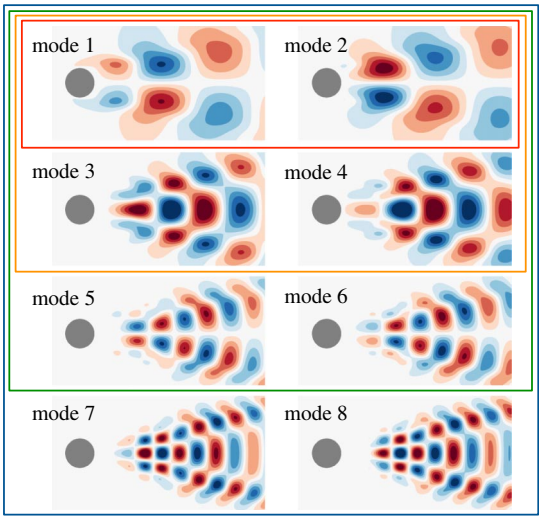

b) POD modes (u velocity)

Fig. 2 POD analysis of cylinder flow: a) original flowfield under study (vorticity shown), b) first eight dominant POD modes, and c) amount of KE of unsteadiness captured by the POD modes.

The aforementioned eight POD modes can capture the flowfield very well for the given data. However, if the flow is perturbed and deviates away from the original flow, additional modes may be needed to represent the perturbed flow. To better capture the perturbed flow, the POD analysis may be repeated with the perturbed flowfield data, or alternative techniques, such as the BPOD analysis [4], may be used (although an adjoint simulation is needed for the latter case). We should keep in mind that the modes extracted from the input flowfield data are optimally determined for the provided data and may not be so for the perturbed flows. The modes may deform when the flow is under the influence of perturbation or actuation. This is an important point to remember if the modal analysis is to be extended or mode-based models are applied to perform flow control.

B. Dynamic Mode Decomposition

We now consider the second data-based approach, the DMD analysis, to study the periodic cylinder wake. For the DMD analysis, the mean subtraction from the snapshots is not necessary, unlike the POD analysis. The findings from the DMD analysis of the cylinder wake are shown in Fig. 3. The dominant mode that arises from the DMD analysis corresponds to a static mode (i.e., DMD eigenvalue $\lambda = 1$), which is the mean flow. The first two rows of Fig. 3a report the real and imaginary parts of the first two oscillatory DMD modes, whereas in the last two rows, we report the magnitude and phase of each of these modes. Note that oscillatory modes appear in complex-conjugate pairs. For brevity, only one element of this pair is plotted. Consider the first oscillatory mode, visualized in different ways within the first column of Fig. 3a. From both the real/imaginary and the magnitude/phase representations, it is evident that this mode captures the top-down asymmetry associated with the von Kármán vortex shedding, which is consistent with the POD analysis. This is not a coincidence, which will be described shortly. The second oscillatory mode is displayed in the second column. The magnitude/phase plots facilitate the distillation of these physical insights. The magnitude plots clearly reveal the active regions of each mode, whereas the phase plot displays the relative phase between spatial regions.

Let us compare the results from the DMD and POD. Unlike the oscillatory DMD modes, all POD modes are real-valued. Because the data here are taken from a limit-cycle oscillation, the POD modes appear in pairs. A side-by-side comparison of the dominant POD modes with the first few oscillatory DMD modes reveals a striking semblance of POD modes 1 and 2 with the real and imaginary parts of DMD mode 1. The same semblance can be found when comparing for POD modes 3 and 4 with the real/imaginary parts of DMD mode 2, and so on for the higher-order modes. Indeed, one can quantify the similarity between these mode shapes by taking an inner product between the DMD mode and a complex vector whose real and imaginary components are formed by the associated POD mode. Performing such an analysis confirms the strong similarity between POD modes and DMD modes for the periodic cylinder wake [37]. Having established this similarity, it now becomes evident that one can plot the magnitude and phase of pairs of POD modes, much in the way that we had done for the DMD modes. Doing so can provide additional interpretable insights into the dynamic significance of these modal structures.

We note that spatial modes from the POD and DMD are not identical to each other, in general. However, they are identical when the flow is periodic in time, as is the case for the cylinder wake at $Re = 100$ considered here. We further note that DMD modes are not necessarily orthogonal to each other, whereas POD modes are. This is an important point to remember when spatial modes are used to form a basis set for use in, for example, reduced-order modeling to be discussed later in Sec. II.D.1.

Although the POD and DMD yield the same spatial modes in the context of the periodic cylinder wake, the DMD offers additional information that the POD is not equipped to provide. Indeed, each dynamic mode consists of spatial information that is embedded in each DMD mode (see Fig. 3a) and temporal information that is embedded in each DMD eigenvalue (see Fig. 3b). Because dynamic modes correspond to the spectral decomposition of a best-fit linear operator that maps one snapshot to the next, the dynamics of each DMD mode comprised only a single oscillation frequency and a growth/decay rate. To determine the oscillation frequency f_i and growth/decay rate g_i of spatial mode i, we can make use of the associated DMD eigenvalue λ_i through $f_i = \angle\lambda_i/(2\pi\delta t)$ and $g_i = \log|\lambda_i|/\delta t$, with δt denoting the uniform sampling increment between snapshot pairs.

In addition to spatial structures (DMD modes) and their simple temporal characteristics (DMD eigenvalues), one can also use the so-called DMD amplitudes to determine the relative contribution of each mode to a particular realization of the system. We note here that different definitions for DMD amplitudes are used throughout the literature. However, two common definitions are 1) DMD amplitudes calculated solely from the initial snapshot, which requires the reciprocal DMD modes; and 2) DMD amplitudes based on all snapshots, which requires a Vandermonde matrix constructed from the DMD eigenvalues. For simplicity, we make use of the former definition in Fig. 3b.

A key lesson to take away from the analysis of a cylinder wake is that the data-collection step is an important consideration. Although one may have access to simulation or experimental data from wake start-up through the periodic evolution on the limit cycle, one rarely

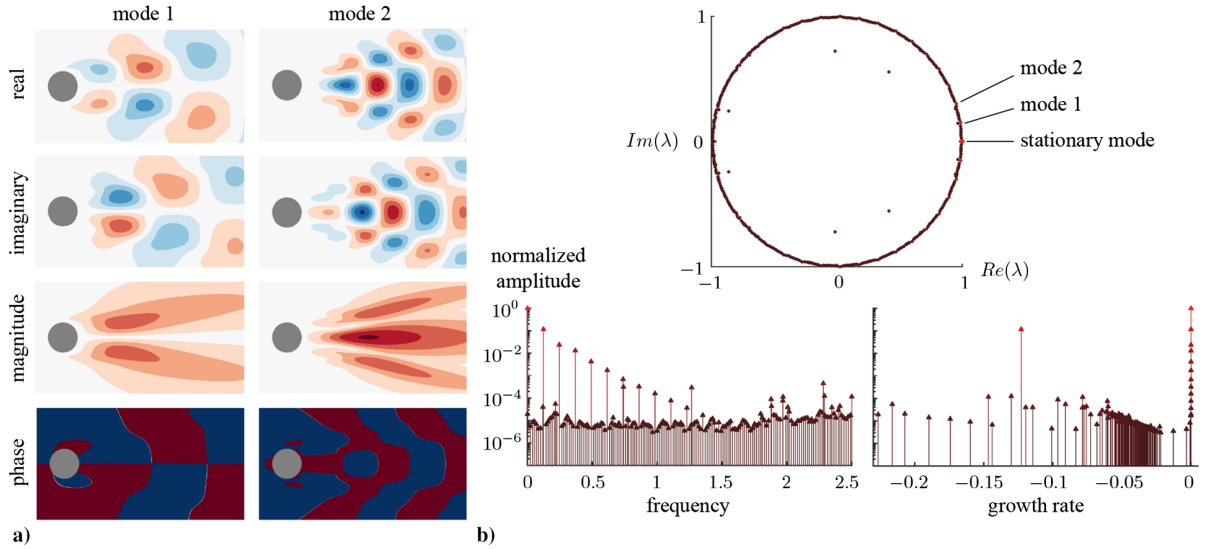

Fig. 3 DMD analysis of cylinder flow: a) the first and second DMD modes with their real, imaginary, magnitude, and phase distributions; and b) DMD eigenvalues representing the growth rates and frequencies.

benefits from "throwing" DMD or another modal-analysis technique at this full data set when particular physical questions are of interest. We can consider the study by Chen et al. [37], in which the dynamics of a cylinder wake are first split into three distinct regimes: near-equilibrium linear dynamics, post-Hopf bifurcation transient dynamics, and periodic limit-cycle dynamics. In performing their analysis, care is taken to consider only snapshots from each of these three regimes independently. Not doing so would contaminate the results of the modal analysis and would arguably lose the interpretability that was being sought. A similar procedure was performed by Bagheri [38]. In that work, too, the evolution of the cylinder wake was divided into four intervals of interest, each associated with a different timescale. Although the cylinder wake is a commonly studied and fairly well-understood flow, both of these works demonstrated how supplementary signals, such as force response data (i.e., lift in [37] and drag in [38]), can be used to delineate between intervals of flow evolution that should be treated separately. By collecting snapshots from these distinct intervals, we can be better equipped to uncover dynamically relevant features and to better understand the dynamic processes underlying the fluid flow. Indeed, in our preceding analyses of the cylinder wake, we ensured that data were only collected once the wake had reached the limit-cycle state.

Finally, it is important to highlight a practical caution for users who are interested in conducting a DMD analysis of experimental data sets. DMD has been observed to exhibit sensitivities [39] and has been shown to yield biased results [40,41] when the snapshot data under consideration possess measurement uncertainties (e.g., due to sensor noise). Thus, users are strongly encouraged to consider noise-robust variants of DMD when analyzing experimentally acquired data sets [40–42].

C. Linear Global Stability Analysis

In the preceding discussions, we used the data-based techniques to study the modal structures generated in the wake of a cylinder. In this section, we will obtain modal structures directly from the linear evolution operator of the Navier–Stokes equations. To examine the cause of unsteadiness in the flow, we resort to a stability analysis. There are two types of stability analyses that can reveal the characteristics of flow instabilities: local and global stability analyses. We focus here on the latter approach, which is suitable for examining instabilities that have global coupling and coverage over the domain of interest. The main difference between global stability analysis [11,12] and the data-based modal-analysis techniques discussed earlier (POD and DMD) is that the global stability analysis requires access to the base flow and the linearized Navier–Stokes operator based on a numerical discretization (e.g., finite difference, finite volume, or spectral method code), whereas the data-based methods do not.

For the global stability analysis, we need the base flow $\overline{\boldsymbol{q}}$ about which to linearize the Navier–Stokes equations. The base state $\overline{\boldsymbol{q}}$ should be the stable or unstable steady-state solution (equilibrium state). See the first overview paper on how to find these states [1]. By decomposing the state variable $\boldsymbol{q}$ into the base state and a perturbation $\boldsymbol{q}'$ (i.e., $\boldsymbol{q} = \overline{\boldsymbol{q}} + \boldsymbol{q}'$), we arrive at the linearized Navier–Stokes equations in discrete form:

$$\frac{\mathrm{d}\boldsymbol{q}'}{\mathrm{d}t} = L_{\overline{\boldsymbol{q}}}\boldsymbol{q}' \tag{1}$$

in which the linear operator $L_{\overline{\boldsymbol{q}}}$ is dependent on the base state $\overline{\boldsymbol{q}}$. By expressing the small perturbation $|\boldsymbol{q}|' \ll |\overline{\boldsymbol{q}}|$ as $\boldsymbol{q}'(\boldsymbol{x}, t) = \hat{\boldsymbol{q}}(\boldsymbol{x})\exp(i\omega t)$, we arrive at

$$L_{\overline{\boldsymbol{q}}}\hat{\boldsymbol{q}} = i\omega\hat{\boldsymbol{q}} \tag{2}$$

This equation casts the stability analysis of the flowfield in terms of an eigenvalue problem. The eigenvalue $i\omega$ reveals the growth/decay rate $\mathrm{Im}(\omega)$ and frequency $\mathrm{Re}(\omega)$ of each spatial eigenvector $\hat{\boldsymbol{q}}$ that is found from this analysis. Thus, we can solve this eigenvalue problem for the dominant eigenvalues and the corresponding eigenvectors to determine the spatial profiles of the instabilities. Alternatively, one can also time integrate Eq. (1) to determine the dominant mode, as an initial value problem. Note also that the construction of the eigenvalue problem for the linear stability analysis used here is standard, but leads to a reversal of roles in the real and imaginary components of eigenvalues when compared to the DMD analysis. Although it is possible to consider the use of a time-averaged (or ensemble-averaged) state as the base flow, the linear stability analysis would not hold, because such state in general is not an equilibrium state. However, the use of a time-averaged base flow may provide some insights as a model, and is used as a precursor to examine the stability property for its resolvent analysis [43] (see other flow examples as follows).

Now, let us consider the application of the linear global stability analysis to cylinder wakes. One of the important insights that can be gained from this analysis is the onset of the wake instability (i.e., the von Kármán shedding), which appears at a critical Reynolds number of $Re_{\mathrm{crit}} \approx 46$. The onset of instability can be identified when the eigenvalues from the stability analysis cross over from the stable to the unstable complex plane, as the Reynolds number Re increases beyond its critical value Re_{crit}. The appearance of this type of instability is called the Hopf bifurcation. We compiled the critical Reynolds numbers, in which the flow is observed to initiate the von Kármán shedding, in Table 2. Included are the critical Reynolds numbers found from careful experiments performed by Taneda [44] and Strykowski and Sreenivasan [45]. On the numerical side of the studies, the global stability analysis performed by Zebib [46] and Jackson [47] have predicted the critical transitions well. Here, we take a broad definition of global stability analysis, especially for papers from earlier stability studies when computational resources were limited. In most of the earlier studies, the modes are not reported, but the eigenvalues are reported in detail. More recently, the stability modes of the cylinder wake at $Re = 50$ have been examined by Abdessemed et al. [48] in a broader context. What is striking from their analysis is the resemblance of the modal shapes between the energetic mode (such as the dominant POD mode shown earlier) and the stability mode. This observation suggests that the instability in the flow causes the wake to oscillate, resulting in the emergence of the von Kármán shedding in the full nonlinear flow. Because the Reynolds number considered in this case is near the bifurcation point of Re_{crit}, the mode shapes of the dominant instability and that of the POD analysis are expected to be similar [49].

Table 2 Compilation of transition Reynolds numbers determined from experiments and stability analyses

Transition	References	Re_{crit}	St_{crit}	Analysis
von Kármán shedding (2-D)	Taneda [44]	45	— —	Experimental
	Provansal et al. [50]	47	0.12	Experimental
	Strykowski and Sreenivasan [45]	46	0.12	Experimental/Numerical
	Zebib [46]	45	0.11–0.13	Stability
	Jackson [47]	46.184	0.138	Stability
Mode A (3-D)	Williamson [51,52]	170–180	— —	Experimental
	Barkley and Henderson [53]	189	— —	Stability
Mode B (3-D)	Williamson [51,52]	230–260	— —	Experimental
	Barkley and Henderson [53]	259	— —	Stability

The linear global stability analysis can be further extended to periodic base states through Floquet analysis [1]. Through such an extension, we can determine the appearance of three-dimensional (3-D) instabilities known as modes A and B, which appear at $Re_A \approx 189$ and $Re_B \approx 259$, respectively [51,52]. Barkley and Henderson [53] and Abdessemed et al. [48] have examined such transitions carefully using stability analysis. We append the theoretical prediction of eigenvalues from the stability analysis in Table 2. The visualizations of the 3-D A and B modes, although not shown here, can be found in [53], which agree well with the dye visualizations presented in [52]. With the identification of the 3-D stability modes, we can observe the regions from which 3-D instabilities are given birth. We also note in passing that we can further consider modal structures responsible for transient growth, as reported by Abdessemed et al. [48].

D. Flow Modeling

1. *Galerkin Modeling*

We have now seen that the POD modes determined from the snapshots can represent the flowfield accurately with remarkable reduction in dimensionality. Instead of requiring a large number of grid points to represent the flow [$n = \mathcal{O}(10^5$–$10^6)$], we can simply reconstruct the flowfield using a small set of POD modes. In the case of a laminar cylinder flow, eight modes can capture the unsteadiness very well, as discussed earlier. Using the low-dimensional representation of the flowfield with POD modes, we can model the dynamics of the flowfield. Here, we present this reduced-order modeling technique based on the Galerkin projection approach [2,54,55]. This approach can provide a small set of ordinary differential equations (ODEs) in terms of the POD coefficients $\boldsymbol{a} \in \mathbb{C}^r$, in which $r \ll n$, to describe the dynamics of the flow.

Let us consider the velocity field to be expressed as a superposition of the POD modes:

$$\boldsymbol{u}(t,\boldsymbol{x}) = \boldsymbol{\varphi}_0(\boldsymbol{x}) + \sum_{j=1}^{r} a_j(t)\boldsymbol{\varphi}_j(\boldsymbol{x}) \tag{3}$$

in which $a_0 = 1$ and $\boldsymbol{\varphi}_0$ represents the mean field. We append a_0 to the coefficient vector $\boldsymbol{a}$ for ease of notation. We substitute this series into the incompressible Navier–Stokes equations, and found that

$$\frac{\partial}{\partial t}\sum_{j=0}^{r} a_j(t)\boldsymbol{\varphi}_j(\boldsymbol{x}) + \sum_{j=0}^{r} a_j(t)\boldsymbol{\varphi}_j(\boldsymbol{x}) \cdot \nabla \sum_{k=0}^{r} a_k(t)\boldsymbol{\varphi}_k(\boldsymbol{x}) = -\nabla p + \frac{1}{Re}\nabla^2 \sum_{j=0}^{r} a_j(t)\boldsymbol{\varphi}_j(\boldsymbol{x}) \tag{4}$$

$$\nabla \cdot \sum_{j=0}^{r} a_j(t)\boldsymbol{\varphi}_j(\boldsymbol{x}) = 0 \tag{5}$$

The second equation is the continuity equation, which is automatically satisfied by each and every POD mode. Hence, we only need to consider the momentum equation. To project these dynamics onto the POD modes, we take an inner product of the preceding equation with $\boldsymbol{\varphi}_i(\boldsymbol{x})$, which yields

$$\frac{\mathrm{d}a_i}{\mathrm{d}t} = \sum_{j=0}^{r} F_{ij}a_j + \sum_{j=0}^{r}\sum_{k=0}^{r} G_{ijk}a_j a_k \tag{6}$$

in which $F_{ij} = -Re^{-1}\langle\boldsymbol{\varphi}_i, \nabla^2\boldsymbol{\varphi}_j\rangle$ and $G_{ijk} = -\langle\boldsymbol{\varphi}_i, \boldsymbol{\varphi}_j \cdot \nabla\boldsymbol{\varphi}_k\rangle$ for $i = 1, \ldots, r$. To arrive at the aforementioned model, we used the orthogonality property of POD modes (i.e., $\langle\boldsymbol{\varphi}_i, \boldsymbol{\varphi}_j\rangle = \delta_{ij}$). From the initial condition for the temporal coefficients $a_i(t_0) = \langle\boldsymbol{u}(t_0,\boldsymbol{x}), \boldsymbol{\varphi}_i(\boldsymbol{x})\rangle$, we can now simply integrate these ODEs to predict the dynamics of the modes. To reconstruct the full flowfield, we simply use Eq. (3). The pressure gradient term drops out from the Galerkin model due to the boundary condition for most flows. Extensive discussions on the treatment of the pressure term and its influence on the model are provided by Holmes et al. [2] and Noack et al. [56]. Modeling efforts by incorporating the pressure POD modes have also been considered to account for the pressure effects [57].

For modeling the cylinder wake, Deane et al. [58] noticed that the use of only four POD modes results in a slow growth of the wake oscillation amplitudes without bounds. However, the ROM with six POD modes improved the accuracy of the model. Deane et al. made a couple of important observations. First is the validity of the ROM modes; for a fixed Reynolds number, the model predicts the behavior of the flow well. However, the use of the mean field and the POD modes from one Reynolds number does not appear to accurately extend to other Reynolds numbers. The second observation is the accuracy of the model over a long time frame. These POD-based ROMs that predict the dynamics well for a short duration can deviate over a long time.

Noack et al. [56] noted the importance of the base flow, and constructed a POD-based ROM that can capture transients from an unstable equilibrium to an asymptotic shedding state (limit-cycle oscillation). In addition to the POD modes obtained from the flowfield data, they supplemented the set of POD basis with the shift mode $\boldsymbol{\varphi}_\Delta$. This additional shift mode amounts to the difference between the mean flow and the equilibrium state, with the modal components projected out, such that

$$\boldsymbol{\varphi}_\Delta = \frac{\boldsymbol{\varphi}_\Delta^b}{\|\boldsymbol{\varphi}_\Delta^b\|}, \quad \text{in which } \boldsymbol{\varphi}_\Delta^b = \boldsymbol{\varphi}_\Delta^a - \sum_{i=1}^{r}\langle\boldsymbol{\varphi}_\Delta^a, \boldsymbol{\varphi}_i\rangle\boldsymbol{\varphi}_i$$
$$\text{and } \boldsymbol{\varphi}_\Delta^a = \boldsymbol{\varphi}_0 - \boldsymbol{u}_s \tag{7}$$

Here, $\boldsymbol{u}_s$ is the steady-state solution to the Navier–Stokes equations. By adding this shift mode to the set of basis functions, the Galerkin-based ROM can be improved to model the transient dynamics well. Such prediction is generally difficult without the shift mode. This model with the shift mode can capture the transient effects with only three modes (shift, first, and second modes), which is a significant reduction in the dimension to describe the emergence of wake instability. Shown in Fig. 4 are the POD-based Galerkin model results compared with the full DNS. Shown on the left are the three- and nine-mode results using the approach of Noack et al. [56].

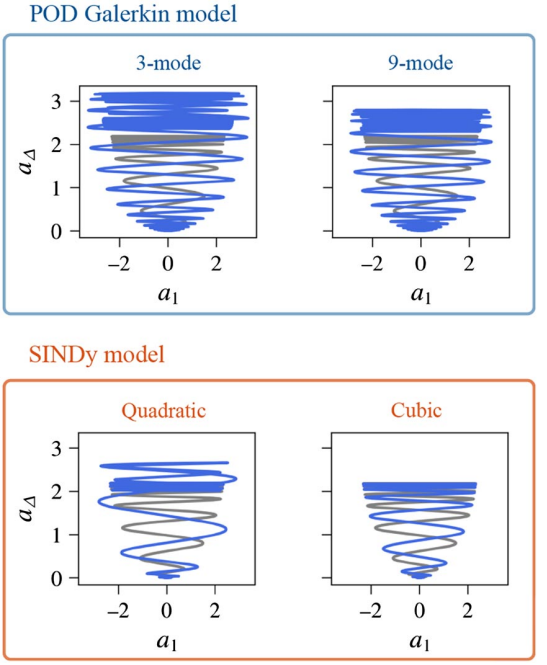

Fig. 4 Galerkin projection and SINDy models for cylinder flow at $Re = 100$; the coefficients capture the transient dynamics of cylinder flow developing the von Kármán shedding instability from the unstable steady state at the bottom of the paraboloid; shown are reference (gray) and model (blue) trajectories. (Reprinted with permission from Cambridge University Press.)

The present discussion on the Galerkin projection model was based on the use of orthogonal POD modes. However, a set of nonorthogonal modes, such as the DMD modes, can be used instead. The resulting model for nonorthogonal modes would include additional terms, yielding a Petrov–Galerkin model. It is also possible to introduce adjoint modes to use bi-orthogonality to derive an ROM [59]. Another approach is to incorporate concepts from network science and machine learning to construct a modal-network model [60].

Despite the success of the Galerkin projection, there are a number of practical issues that arise when using it to develop ROMs. First, the expansion in Eq. (3) is typically truncated at a low-order $r \ll n$ to develop an efficient model in terms of a few dominant coherent structures. However, truncating the modal expansion removes the effects of low-energy modes, which might be dynamically important. When these terms are removed, subtle imbalances appear in the quadratic nonlinearities, which often eventually lead to long-term instability. It is possible to correct for these issues by enforcing energy-preserving symmetries in the quadratic terms in the Galerkin projection process [55,61–63]. It may also be the case that, for complex, multiscale dynamics, the flow structures are not adequately captured in a low-dimensional linear subspace. Because Galerkin projection models typically scale with $\mathcal{O}(r^3)$, these models quickly become more expensive than the original full-order model without further measures. Finally, POD modes generally deform with changing flow conditions and geometries, so that a given model derived at one flow condition may have restricted utility for other conditions. A number of these issues will be discussed in the next section and also in the outlook in Sec. VI.

2. *Sparse Identification of Nonlinear Dynamics*

As an alternative to Galerkin projection of the governing equations onto an orthogonal POD basis, it is possible to identify a nonlinear dynamic system in this subspace by data-driven regression. In particular, the sparse identification of nonlinear dynamics (SINDy) algorithm [64] may be used to discover a low-order model based on time-series data of the POD coefficients as the system evolves. Given a vector of POD coefficients, $\boldsymbol{a}$, it is possible to represent the right-hand side of the dynamics of $\boldsymbol{a}$ as a linear combination of basis functions $\theta_j(\boldsymbol{a})$ in a library:

$$\frac{\mathrm{d}\boldsymbol{a}}{\mathrm{d}t} = \boldsymbol{f}(\boldsymbol{a}) \approx \sum_{j=1}^{p} \theta_j(\boldsymbol{a})\xi_j \tag{8}$$

The SINDy algorithm seeks a sparse vector of coefficients $\boldsymbol{\xi}$, indicating that as few terms $\theta_j(\boldsymbol{a})$ are active in the dynamics as possible. This is achieved via modern methods in sparse regression, and helps to ensure that the resulting models are both interpretable. This approach was recently extended to model fluid systems by Loiseau and Brunton [65] and Loiseau et al. [66]. It was shown that known constraints can be incorporated in the SINDy regression framework, such as energy-conserving constraints on the quadratic nonlinearities for incompressible flows [65]. In particular, it is known that a particular skew-symmetry in the quadratic nonlinearities gives rise to energy conservation in incompressible flows, and it is possible to enforce this model structure in the sparse regression procedure via Lagrange multipliers. In general, there is a growing effort, especially in fluid mechanics, to incorporate known symmetries, constraints, and conservation laws into various machine learning algorithms [67].

Furthermore, unlike in the Galerkin projection, in which the nonlinear terms in the ROM reflect those in the governing equations, in SINDy, it is possible to include higher-order nonlinearities, which may serve to account for the effects of truncated terms in the POD expansion. A comparison of SINDy models and the standard Galerkin projection is shown in Fig. 4, in which a SINDy model with cubic nonlinearities nearly perfectly captures the true dynamics. This approach was later shown to be effective on sensor-based coordinates, such as lift and drag measurements, removing the need for full-state data and POD analysis, and bypassing the mode deformation associated with changing flow conditions. These ROMs can be used to stabilize the wake shedding for drag reduction [68].

III. Wall-Bounded Flows

Wall-bounded flows are one of the most ubiquitous flows that arise in the study of fluids systems. Wall-bounded shear flows have important differences from those considered in Sec. II, which may exhibit oscillator-type dynamics characterized by a single dominant frequency and length scale. In contrast, wall-bounded flows at a sufficiently large Reynolds number can exhibit energetic structures at a broad range of lengthscales and timescales. Wall-bounded configurations, including channel, pipe, Couette, and boundary-layer flows, share similarities in terms of both flow physics and analysis methods. Here, the focus will be on flow through a uniform channel with infinite extent in the streamwise and spanwise directions. The assumption of spatial homogeneity assumed here is common in modal analysis, as spatial Fourier modes can be used to represent these spatially homogenous directions [2]. However, this simplification can come at the cost of inefficiencies for identifying and modeling localized or spatiotemporally developing structures. Nonetheless, we adopt this simplification, as the assumption of spatial homogeneity typically reduces the amount of data required for data-driven methods, and reduces the computational requirements for operator-based decompositions.

Famously, a laminar flow in a channel becomes linearly unstable at a Reynolds number (based on channel half-height) of $Re = 5772$, as first computed precisely by Orszag [69]. However, transition to turbulence may be triggered and sustained at a much lower Reynolds number than predicted by this linear (modal) stability analysis. Indeed, the linear dynamics predict that perturbations about the laminar equilibrium state can exhibit a significant growth prior to subsequent decay—a phenomenon known as transient energy growth, which can be studied using a nonmodal stability analysis [70]. Transient energy growth is commonly attributed to the high degree of nonnormality of the linearized Navier–Stokes operator, which is observed in numerous wall-bounded flows. The purpose of this section is to demonstrate how modal-decomposition techniques may be applied to this class of flows, and to summarize and compare typical results from each method. We will not attempt to provide a comprehensive analysis of every aspect of the flow physics, nor a complete summary of the substantial body of prior work using modal-decomposition techniques on this class of problems. In this section, we will first consider in detail the case of a stable linearized channel flow in Sec. III.A, before discussing how similar methods may be extended to study turbulent (Sec. III.B) and spatially developing (Sec. III.C) wall-bounded flows.

A. Linearly Stable Laminar Channel Flow

We consider a system at a half-height-based Reynolds number of $Re = 2000$, as illustrated in Fig. 5. This section will focus only on the dynamics with streamwise and spanwise wave numbers of $k_x = 0.25$ and $k_z = 2$. The dynamics are linearized about a laminar equilibrium state (i.e., a parabolic streamwise velocity profile). This simple example highlights certain features of wall-bounded flows, and serves as a test bed to compare many of the modal-decomposition methods considered in this paper. There are many references that give a more comprehensive treatment of this system [71,72] with some of the analysis presented here similar to that described in [4,70,71,73,74]. For this example, we formulated the problem in terms of the Orr–Sommerfeld and Squire equations, and show the results using the wall-normal velocity and vorticity.

In contrast to the approach taken in Sec. II, we first consider an operator-based analysis of this system, before progressing to a data-driven analysis (in which the choice of data will be informed by the results of the operator-driven analysis). To start with, we consider the stability properties of the linear operator for this system. In addition to studying the asymptotic stability (governed by the eigenvalues or spectrum of the operator), we also consider the pseudospectrum, which can be viewed as a measure of how close a given point in the complex plane is to being an eigenvalue. More formally, the

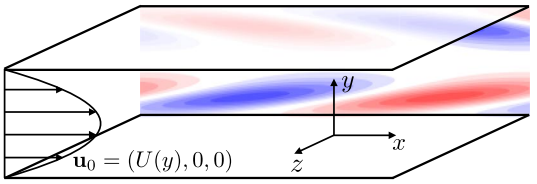

Fig. 5 Channel geometry superposed with the mean profile and a 2-D slice of the leading resolvent response mode for this system at $Re = 2000$, $k_x = 0.25$, $k_z = 2$, and $c_r = 0.578$.

ϵ-pseudospectrum of a linear operator L is the set of values z in the complex plane satisfying the following equivalent conditions for a given ϵ:

1) $\|L\boldsymbol{q} - z\boldsymbol{q}\| \leq \epsilon$ for some pseudoeigenvector $\boldsymbol{q}$;
2) $(L + E)\boldsymbol{q} = z\boldsymbol{q}$ for some perturbation operator E, with $\|E\| \leq \epsilon$; and
3) $\|(zI - L)^{-1}\| \geq \epsilon^{-1}$.

The operator $(zI - L)^{-1}$ is the resolvent operator associated with L for a given z, with the associated resolvent norm $\|(zI - L)^{-1}\|$. Detailed discussions of pseudospectral theory in the context of fluid flows are offered in [70,75].

The eigenvalue spectrum for this stable system, along with contours of the pseudospectra for various values of ϵ, are shown in Fig. 6a. By Squire's theorem, the system would become less stable if the spanwise wave number were reduced to 0. Even when the system is asymptotically stable, the nonnormal nature of the associated linear operator renders it susceptible to both the transient energy growth over finite time horizons and the high amplification of external disturbances/inputs. Note that, in the case of a normal operator, the ϵ-pseudospectrum consists of the union of concentric disks of radius ϵ about each eigenvalue. For nonnormal operators, such as that considered in Fig. 6a, the ϵ-pseudospectrum can be far larger and can deform away from being a union of concentric disks. In this case, the union of concentric disks of radius ϵ about each eigenvalue instead gives a lower bound for the ϵ-pseudospectrum, with an upper bound given by the equivalent union of disks of radius $\kappa\epsilon$, in which κ is the condition number of the operator.

The maximum amplification of the system to a single-frequency input is given by the norm of the resolvent operator associated with the linear system for that frequency, which is equivalent to the contours of the pseudospectra plotted in Fig. 6a. We are typically interested in purely oscillatory disturbances, which correspond to the dashed line in Fig. 6a. The optimal disturbance and response at a wave speed ($c_r = \omega/k_x = 0.578$) leading to maximum amplification for this system are shown in Fig. 6b (which correspond to the filled circle in Fig. 6a). A contour plot through a spanwise-constant slice of the domain of the resolvent response mode for these parameters is also shown in Fig. 5. This optimal disturbance and response may be obtained, respectively, from the leading right and left singular vectors of the resolvent operator associated with this frequency.

The initial and final conditions of the trajectory giving maximal energy growth for this system are shown in Fig. 6b. The maximum energy is attained by the system at a time horizon $\tau = 58$, in which the initial and final conditions giving maximum energy growth can be obtained from the leading right and left singular vectors of the finite time propagation operator $\exp(L\tau)$. The evolution of the energy of the system for this trajectory is shown in Fig. 7. Note that transient growth may be formally related to the pseudospectral/resolvent analysis via the Kreiss constant [76], as discussed in the context of channel flow in [70,75].

Thus far, we have analyzed this system through a study of the operator itself. We now give attention to data-driven modal-decomposition methods. We will focus on data collected on the trajectory giving the largest energy growth, with an initial condition as shown in Fig. 6b. Performing DMD on this trajectory (collected with a time step $\delta t = 0.01$) gives eigenvalues as shown by the open circles in Fig. 6a. We observe that DMD identifies some, but not all, of the eigenvalues of the system. Physically, DMD identifies those modes that are active in the given data set. Because DMD is a data-driven method, it cannot take advantage of rescaling and normalization that are typically applied when using iterative methods, such as an Arnoldi procedure [6]. Note in particular that, for this system, the eigenvalues near the intersection between the eigenvalue branches are particularly susceptible to perturbation, which is again related to the nonnormality of the system. Furthermore, although the operator identified using DMD shares only a subset of the true eigenvalues of the full operator, it is able to reconstruct the data that were used for its identification. This is not surprising, because the underlying dynamic system is linear.

The leading POD modes identified from this data set are shown in Fig. 7. We observed that the leading POD modes are dominated by the wall-normal vorticity component, and also that only a few modes are required to account for the vast majority of the energy present in the data. We may use these modes as a basis for projection of the governing equations to obtain a ROM for the system dynamics. Note that this is the same procedure presented in Sec. II.D.1, but here, we consider the simpler case of a linear system. In particular, if the basis of the POD modes to be used for projection is given by the columns of

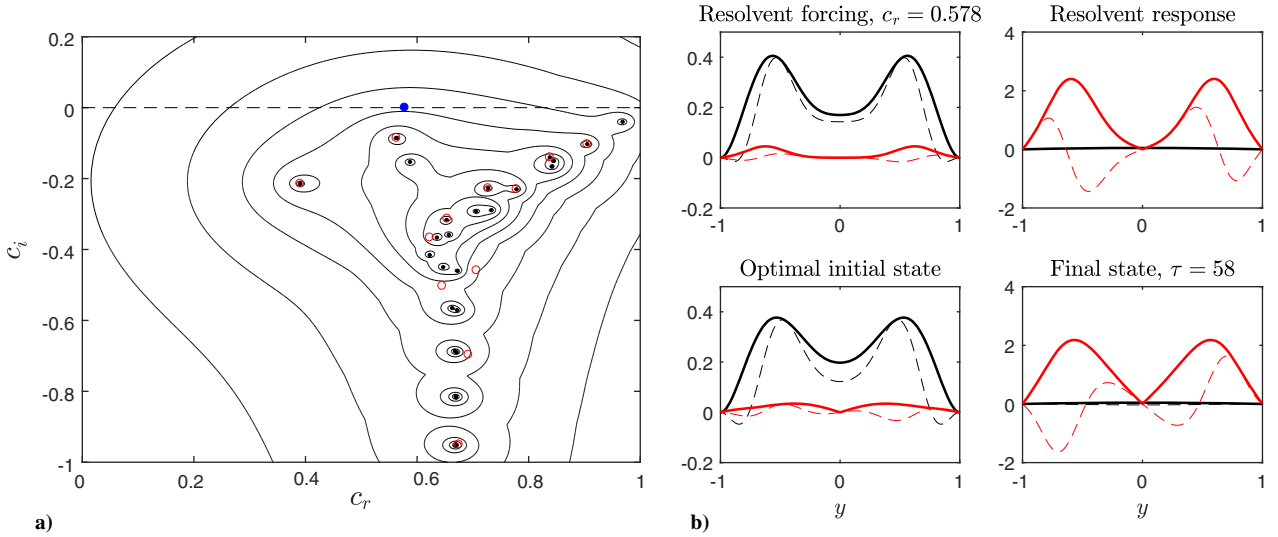

Fig. 6 a) Eigenvalues (expressed as a complex growth rate $c = \lambda/k_x$) and contours of the pseudospectra for channel flow with $Re = 2000$, $k_x = 0.25$, and $k_z = 2$; DMD eigenvalues identified for a trajectory giving optimal transient growth are shown with unfilled circles, whereas the filled circle at $c_r = 0.578$ represents the real frequency corresponding to maximum resolvent norm; b) leading resolvent forcing and response modes corresponding to a wave speed ($c_r = 0.578$) leading to maximum amplification, and initial and final (maximally amplified) states along a trajectory leading to maximal energy growth; all modes are scaled to be of unit norm, with black and red lines corresponding to wall-normal velocity and vorticity fields, and solid and dashed lines representing the magnitude and real component of these fields.

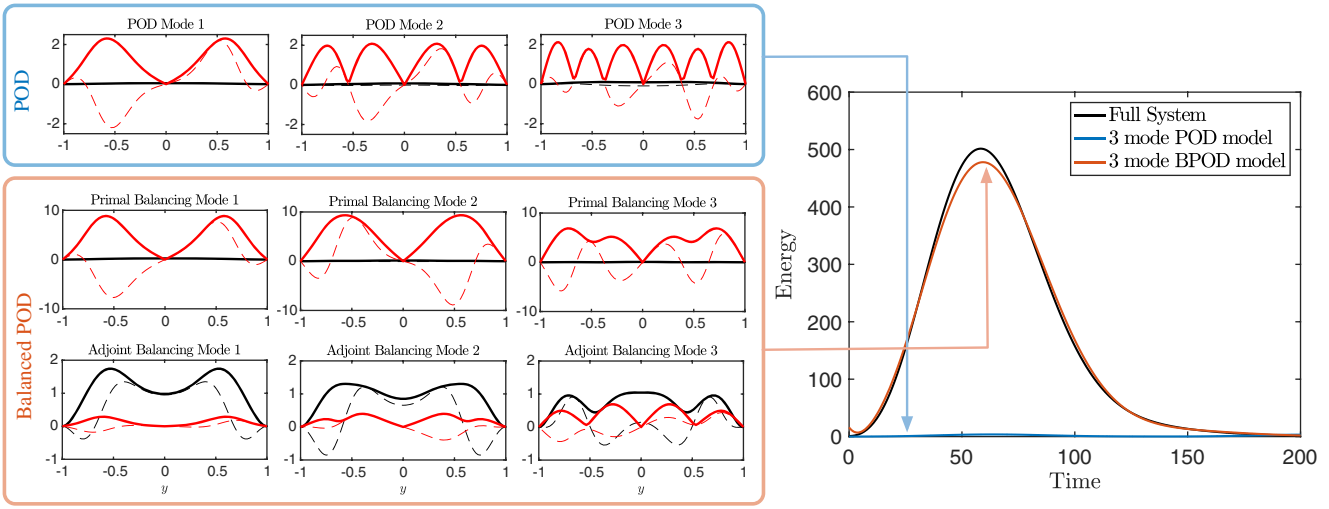

Fig. 7 Development of POD- and BPOD-based models; shown on the left are POD, and balancing primal and adjoint mode amplitudes (solid lines) and real components (dashed) for the wall-normal velocity (black) and vorticity (red); shown on the right is the evolution of the energy of the system along a trajectory leading to maximal finite time energy growth, compared with predictions from the three-mode POD and BPOD models.

a matrix Φ, then the reduced-order operator $\tilde{L}$ can be obtained from the full operator L by

$$\tilde{L} = \Phi^* L \Phi \tag{9}$$

in which Φ^* is the adjoint of Φ. Performing such a projection using the first three POD modes gives a model that poorly reconstructs the trajectory of the data, as shown in Fig. 7.

This can be understood by the fact that the total energy of the system, and thus, the leading POD modes, is dominated by the wall-normal vorticity component, yet the initial condition used contains a substantial wall-normal velocity component. Note in particular that the leading three POD modes account for less than 4% of the energy of the initial condition. However, if five modes are used instead, this measure exceeds 95% and an accurate ROM can be obtained. This demonstrates that total energy content is often not the most important factor for identifying a basis for projection of the full governing equations, because there may be features that are dynamically important, even though they are low in energy.

For a linear system with a given set of system inputs and outputs, a projection-based ROM that best preserves the input/output dynamics may be obtained through a balanced truncation [77]. A balanced truncation finds a compromise between system observability and controllability, which are analogous to the total energy content and initial conditions for the system considered here (if one considers the initial conditions as the input matrix for a single-input linear state-space system). Rather than using a single set of modes to form a basis for projection as in Eq. (9), we obtain a ROM by finding separate subspaces that define the basis upon which the reduced dynamics evolve (basis vectors for which can be assembled as columns of a matrix Φ) and the direction of the projection onto that subspace (with a basis given by the columns of Ψ, which are bi-orthogonal to those of Φ). The reduced linear operator is then related to the full system by

$$\tilde{L} = \Psi^* L \Phi \tag{10}$$

with system inputs and outputs appropriately projected. We refer to the columns of Φ and Ψ as the primal and adjoint modes, respectively.

Although it is feasible to perform a balanced truncation directly for the simple system considered here, it can become difficult or infeasible for large systems. BPOD [4] gives a means to perform an approximate balanced truncation from impulse response data from the forward and adjoint systems (which have state propagation operators given, respectively, by L and L^*). As seen in Fig. 7, applying this method gives a three-mode model that accurately captures the trajectory of the data, unlike the POD model. For the BPOD model, we apply output projection [4,78] to reduce the dimension of the full-state output down to just seven variables. The POD model projects the governing equation onto a subspace along a direction orthogonal to the subspace, whereas the BPOD computes a direction of projection that best preserves the dynamics of the system. We show in Fig. 7 the primal modes onto which the dynamics are projected and the adjoint modes defining the direction of projection. Note in particular that the primal modes are dominated by the wall-normal vorticity (as are the POD modes), whereas the adjoint modes have a substantial contribution from the wall-normal velocity. This allows for a projection that retains a sufficient dynamically important content of the full system to give an accurate ROM.

The possibility of capturing input/output dynamics using modal-analysis techniques has made balanced truncation and BPOD attractive for active flow-control synthesis. Indeed, modal analysis can guide the choice of actuation and sensing, and can also inform designs of open-loop control strategies [79,80]. Further, modal-analysis techniques can be tailored to and leveraged for feedback flow-control synthesis. Within the context of channel flow control, numerous model-reduction strategies have been developed around modal-decomposition techniques (e.g., global mode truncation [81] and input/output modeling [82–84]). Recent efforts have demonstrated that a model-reduction approach needs to be selected and tailored carefully with respect to the control objective [83,84]. For example, within the context of transient energy growth reduction, the performance of feedback controllers designed on ROMs can be quite sensitive to the parameters used in generating the underlying ROMs [83,84].

Interestingly, the physical and descriptive insights offered by the modal analysis can potentially guide feedback flow-control designs as well, motivating a new perspective for dynamic mode shaping control synthesis, in which the closed-loop spectral properties of a system can be prescribed by an appropriate control action [85]. These same efforts on dynamic mode shaping have recently been used to uncover fundamental performance limitations in commonly employed sensor-based output feedback controllers that are commonly employed in flow-control applications. Indeed, it can be shown that observer-based feedback strategies—in which the flow state is reconstructed from measured sensor outputs, then leveraged for feedback control—can never fully suppress transient energy growth within the context of linearized flows that exhibit transient energy growth in the first place [86]. Furthermore, such strategies have been found to dramatically degrade performance in terms of the worst-case transient energy growth in the linearized channel flow system [80,87]. Alternative output feedback-control strategies have been found to be superior in terms of the worst-case transient energy growth performance. However, most synthesis algorithms suffer from the curse of dimensionality, necessitating the use of ROMs to

make synthesis tractable in flow-control applications. Control-oriented model reduction based on modal decompositions and other systems-theoretic techniques (e.g., robust/$\mathcal{H}_\infty$ modeling [88]) will play an important role in overcoming these hurdles into the future.

B. Turbulent Wall-Bounded Flows

This section will discuss how a number of ideas and methods discussed in Sec. III.A have been applied to turbulent flows, in which spatial homogeneity is assumed in the streamwise and spanwise directions. Operator-based linear analyses of turbulent flows typically consider mean linearized governing equations. Although such analyses are generally not able to predict the exact evolution of trajectories as in the case of linear flow, a substantial insight into the features of turbulent flows can still be gained from consideration of linear operators. A modal linear stability analysis about wall-bounded turbulent mean flows often gives stable eigenvalues [89,90] (although this is not the case for some of the geometries considered in Secs. IV and V). Indeed, the discrepancy between Squire's theorem, whereby the least stable modes are spanwise constant, and observations of the three-dimensionality of both transition mechanisms [91] and structures in fully developed turbulence show the limitations of linear eigenmodes. The combination of a nonnormal system with nonlinear terms of substantial size means that nonmodal properties make considerations of nonnormality particularly important for wall-bounded (or more generally, shear-driven) turbulent flows [70]. Operator-based analyses of turbulent flows have been used in various contexts as a tool to probe, quantify, and explain the physics underlying phenomenological studies of observed structures, such as near-wall streaks [90] and their role in the amplification of streamwise vortices [92], hairpin structures [93], and self-similar structures [94,95].

A particularly fruitful approach for an operator-based modal analysis of turbulent wall-bounded flows, used in several of the aforementioned studies, comes from consideration of the resolvent operator associated with the mean linearized equations [96–98], and in particular, its singular-value decomposition. More generally, the utility of such analysis in fluids arises because the pseudospectrum is often more relevant than the spectrum for understanding typical instability and amplification mechanisms [13,72,75,99,100]. The nonlinear terms appear as a feedback interconnection with the linear resolvent operator within this analysis framework. As such, a gain-based (input/output) decomposition of the linear resolvent operator provides insights regarding the amplification of velocity and pressure modes due to the nonlinear forcing terms [98]. Recently, the resolvent formalism has been extended to study the influence of surface-roughness effects, providing a convenient tool for studying passive flow-control devices, such as, for example, compliant surfaces [101] and spanwise periodic and streamwise-constant riblets [102]. Similar extensions can also be used to design active control strategies [103].

Although the resolvent formalism has become a prominent method for analyzing wall-bounded turbulent flows in recent years, the approach has close connections with other modal-analysis techniques as well. Under the assumption that forcing results in uncorrelated resolvent response-mode expansion coefficients, it can be shown that resolvent response coincides with spectral POD modes [104], providing a connection between operator-based and data-driven modal decompositions. Indeed, POD has a rich history in the study of wall-bounded turbulent flows [2,3,105,106], with the initial approaches being tractable using two-point correlation measurements [105].

Recent investigations have also applied resolvent-based models for state estimation from limited measurements [107,108], and have also leveraged covariance completion techniques to model the nonlinear forcing terms within the resolvent framework as appropriate colored noise processes [109,110]. These recent investigations may offer a convenient set of reduced-complexity models that can guide future investigations on controlling turbulent wall-bounded flows.

C. Spatially Developing Flows

In contrast to fully developed parallel channel flow, the boundary layer over a flat plate grows slowly in the streamwise direction. The boundary-layer thickness grows as $\delta \sim \sqrt{x\nu/U_\infty}$, in which U_∞ is the freestream velocity and ν is the kinematic viscosity. At a sufficiently high Reynolds number, a disturbance generated at an upstream location grows in amplitude as it is transported downstream by the mean flow. Therefore, the flow is globally stable, but is locally convectively unstable. The latter instability refers to the fact that a local stability analysis would yield an unstable system, based on a parallel-flow assumption with the mean profile taken from a particular fixed streamwise position. In the full physical domain with a global viewpoint, however, the growth of perturbations at a fixed streamwise position is only a transient phenomenon, thus rendering the system as asymptotically stable [111].

The characteristic feature of convectively unstable flows is that they behave as amplifiers when externally forced. In particular, external perturbations (e.g., acoustic waves and freestream perturbations) continuously penetrate the boundary layer during a receptivity phase and trigger disturbances [Tollmien–Schlichting (TS) waves or streamwise vortices] that grow as they propagate downstream with the mean flow. If these disturbances reach above a certain threshold in amplitude, they may induce a breakdown to a turbulent flow. The focus of a large number of studies has thus been on transition control that aims to delay the transition process by suppressing the growth of boundary-layer disturbances. Within this context, modal-decomposition techniques have been instrumental for reducing the number of degrees of freedom of the fluid system [typically $\gtrsim\mathcal{O}(10^6)$] to yield a modal-based ROM [typically $\lesssim\mathcal{O}(10^2)$]. Specifically, efficient and small ROMs can be constructed when the input/output dynamics are much simpler than the full spatiotemporal perturbation dynamics. For example, this is the case for feedforward control of TS waves using a few strategically placed actuators and sensors flush-mounted on a flat plate. The output signal from an upstream sensor used to detect propagating disturbances is fed to a suitable controller, which in turn provides an actuation signal (input) that attenuates the measured disturbances through interference.

The construction of modal-based ROMs has been particularly successful using BPOD modes [112,113]. A BPOD basis takes into account the sensitivity to upstream forcing via the adjoint balanced modes. In contrast, the leading POD modes represent the most energetic structures located far downstream, and thus, have little spatial support upstream near the forcing. This makes it difficult to obtain small and accurate Galerkin models of the input/output dynamics. A number of studies have also used the direct and adjoint eigenmodes of the linearized system as an expansion basis to construct ROMs [114]. However, these models quickly become ill-conditioned, as the streamwise separation between consecutive pairs rapidly increases [115]. Although modal-based ROMs have resulted in experimentally viable controllers [116,117], one of their limitations is that they require detailed knowledge of the spatial distribution of the upstream disturbance source (or noise environment). This requirement, which poses a limitation in experimental settings in particular, has resulted in a number of alternative approaches to obtain ROMs based on system identification methods [118].

A number of groups have used modal-decomposition techniques to extract and understand the inherent dynamics of spatially developing flows. However, extraction of temporal dynamics using data-driven methods is a challenging problem in noisy environments. If the system is continuously driven by external noise, the system will, after a transient, reach a statistically steady state, thus causing the collected snapshot data to contain both external driving and inherent dynamics [119]. A DMD analysis performed on such a data set will provide a spectrum with marginally stable eigenvalues, which is in contradiction with the damped spectrum of these systems. However, the DMD modes provide information about spatial inherent dynamics corresponding to a spatial stability analysis.

To illustrate this, let us consider the uniform flow over a flat plate, where a localized harmonic forcing in the wall-normal direction of frequency ω is continuously applied upstream in the boundary layer. An instantaneous snapshot of the streamwise velocity component is shown in Fig. 8a. The growing boundary layer is modulated by periodic forcing. The zeroth, first, and third DMD modes are shown in Figs. 8b–8d. The zeroth DMD mode corresponds to the time-averaged mean flow, which, for this small-amplitude forcing, is very close to the Blasius solution. The first DMD mode corresponds to a

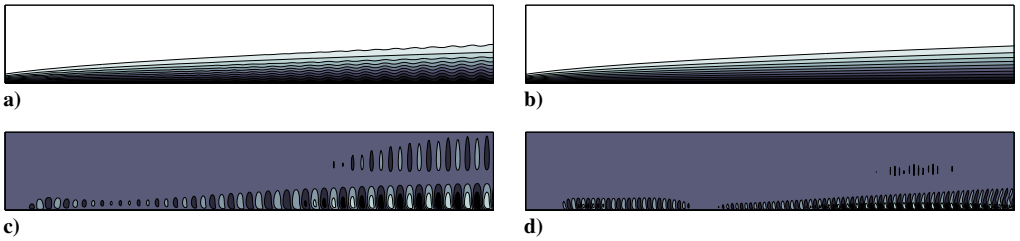

Fig. 8 a) An instantaneous snapshot of the streamwise velocity component of the harmonically forced flat-plate boundary layer with nondimensional frequency $F = 10^6\omega\nu/U_\infty^2 = 120$; the inlet Reynolds number based on the displacement thickness and freestream velocity is $Re_x = U_\infty x/\nu = 30{,}387$ in a 2-D computational box; b–d) the zeroth, first, and third DMD modes (all marginally stable) of the system; c) a TS wave is observed that grows in the streamwise direction between branches I and II at a rate predicted by the local spatial stability analysis.

TS wave, in which the associated DMD eigenvalue λ_j has zero growth rate and a frequency that is equal to the forcing frequency. As mentioned earlier, the zeroth temporal growth rate predicted by DMD is in contradiction with a global spectrum of the system, which predicts a damped system. However, in Fig. 8c, we observed that the amplitude of the DMD mode decays immediately downstream of the location of the forcing before it begins to grow at a particular streamwise location (branch I) until it peaks further downstream (branch II). The spatial locations of branches I and II for this particular forcing frequency correspond to values obtained from the neutral curve of a local analysis of the Blasius boundary layer [71]. The third DMD mode in Fig. 8d corresponds to another TS wave with frequency 2ω generated from nonlinear interactions.

IV. Airfoil Wakes

Flow over an airfoil is another example that attracts great engineering interests in aerodynamic and turbomachinery applications. Modal analysis has examined various aspects of airfoil wakes, including the wake structures [120,121], body geometry [122,123], tip vortex [124–127], aeroacoustics [128–130], and buffeting [131–134]. Key efforts have been placed on mitigating flow separation over an airfoil for performance enhancement and improved safety of aircraft. In this section, we discuss how a modal analysis can be used to study the flow physics over the airfoil and how its insights can be used to develop effective separation-control strategies. In Secs. IV and V, we focus on the excitation of modes to modify the mean-flow profile. Although we can also consider the suppression of modes as a way to control fluid flows, its effectiveness on modifying the flow can be in question for higher-Reynolds-number flows, in which nonlinear effects are strong. On the other hand, excitation can push the flow away from its current state, if successful, and alter the mean-flow profile across a range of Reynolds numbers as some of the examples that follow will show.

A. POD and DMD Analyses

We have discussed the importance of the time window and temporal resolution for the snapshots used in the data-based modal analyses. For high-Reynolds-number separated flows, high temporal resolution is required to capture the shear-layer structures over the airfoil. To accurately capture the wake structure, on the other hand, we need to ensure that the snapshots are adequately collected over a reasonable number of vortex-shedding periods. For turbulent flows, a large number of snapshots in time are needed due to the chaotic nature of the wake dynamics.

The spatial domain for data-based analyses should be based on the physics under examination. If the global snapshots of a high-Reynolds-number separated flow are used to perform POD, shear-layer structures over the separation bubble may only be revealed at high-order modes. This is because POD modes are ranked with respect to the relative energy content, and shear-layer structures usually contain a smaller fraction of energy compared to the wake structure. If the shear-layer structures are of the main interest, we can consider the domain to cover only the separation bubble so that the shear-layer structures can be analyzed with low-rank POD modes. We also note that the same purpose can be served by introducing the spatial window as a weighted function. If DMD is performed, it can automatically separate the shear-layer structures from the wake structures according to their own corresponding frequencies, as each DMD mode holds a single frequency.

A data-based modal analysis on airfoil flows has been shown to be capable of capturing coherent structures at chord-based Reynolds numbers up to $\mathcal{O}(10^5)$ [123,135]. The studies by Ribeiro and Wolf [130] and Ricciardi et al. [136] considered a 3-D data set collected for a turbulent flow over a NACA 0012 airfoil at $Re = 408,000$. Similar to Freund and Colonius [137], their POD analysis considered the use of different norms to reveal the flow structures that are associated with tonal noise. The leading POD modes using the norms based on KE and pressure fluctuation are shown in Fig. 9. The use of these norms reveals similar structures associated with the generation of dominant tonal noise according to the spectral content of their temporal coefficients. However, the POD modes from the second pair (mode 3) exhibit different structures with the use of different norms. The use of the pressure norm uncovers spanwise structures associated with the harmonics of the dominant tone, whereas the KE norm reveals streamwise structures over the airfoil, which do not attribute to the tonal-noise generation. This study highlights the importance of the choice of norms in a POD analysis. It also suggests that the collection of 3-D data set can be necessary even when spatial homogeneity may appear appropriate, as the energetic streamwise structure in mode 3 would not have been revealed if only a spanwise slice of data was considered in the modal analysis.

B. Global Stability Analysis

Global stability analyses of flows over a NACA 0012 airfoil have been performed by Theofilis [138] and Zhang and Samtaney [139]. An example of the spectrum and eigenmodes obtained from Zhang and Samtaney [139] is presented in Fig. 10. Here, unstable equilibrium flows over the airfoil at $Re = 400$ to 1000 are considered as the base states. With the spatial periodicity assumed in the spanwise direction, they adopted the biglobal mode representation $\boldsymbol{q}'(\boldsymbol{x}) = \hat{\boldsymbol{q}}(x, y)\exp(i\omega t + i\beta z)$, in which z is the homogeneous spanwise direction and β is the spanwise wave number. Unstable eigenvalues are found for the base flows at all selected Reynolds numbers, corresponding to the unstable vortex shedding observed in

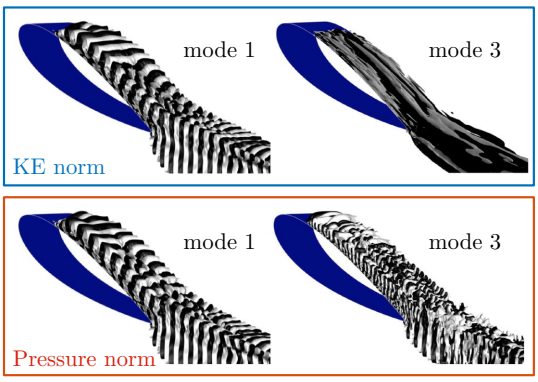

Fig. 9 POD modes obtained with perturbation KE norm (top) and pressure norm (bottom) [130] reveal distinctive structures in the second mode pair (mode 3). (Reprinted with permission from AIP Publishing.)

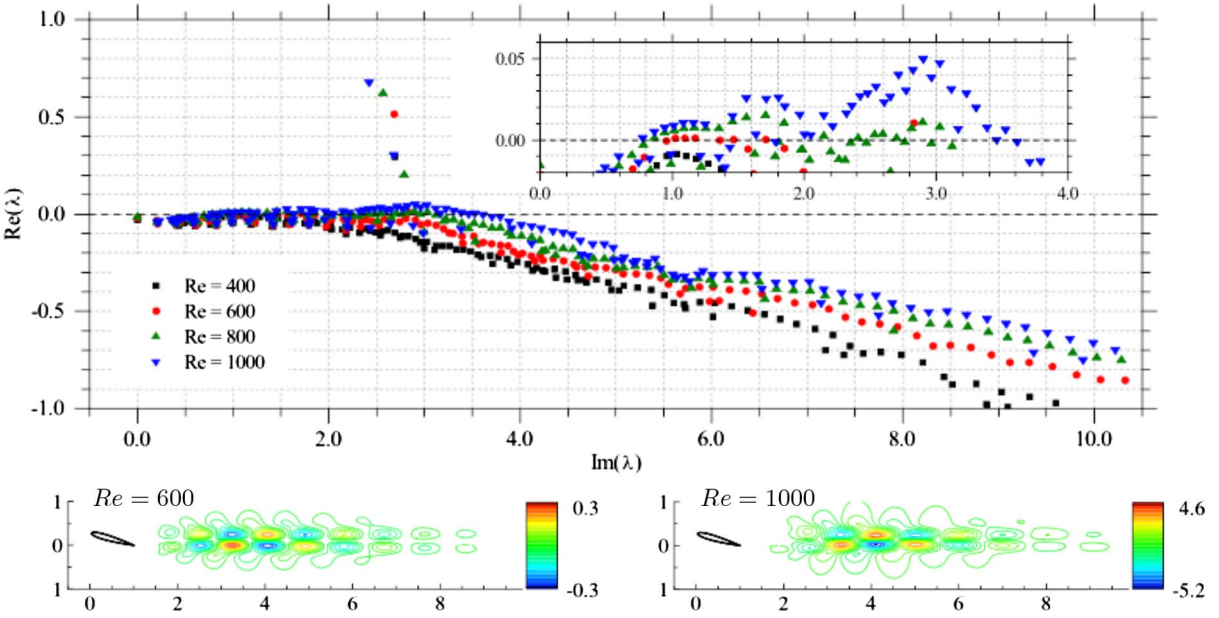

Fig. 10 Spectrum (left) and dominant unstable eigenmodes (right) from the biglobal stability analysis on flows over a NACA 0012 airfoil [139]; results from the spanwise wave number $\beta = 0.0001$ are shown; the streamwise velocity components of the eigenmodes are shown for $Re = 600$ and 1000. (Reprinted with permission from AIP Publishing.)

the companion DNSs. Moreover, the dominant unstable eigenmodes reveal vortex-shedding structures in the pattern of bluff-body wake. These corresponding frequencies determined from the stability analysis agree with the shedding frequencies observed in the DNSs. The destabilizing effect from increasing Reynolds number is also reflected in the increasing growth rates of the eigenvalues.

A global stability analysis can be extended to periodic base flows by incorporating Floquet analysis [53]. The stability of the periodic base flows representing the vortex shedding in airfoil wake has been examined with Floquet analysis by He et al. [140]. In their study, the 3-D instability is treated as a secondary instability that takes place about the 2-D periodic base flow. The stability is determined by the magnitude of the Floquet multiplier, which indicates the growth/decay rate of the 3-D perturbation when propagating with the 2-D periodic base flow. Considering the periodic base flow over the NACA 4415 airfoil at $Re = 500$, two instability modes, as shown in Fig. 11, appear at the spanwise wave numbers $\beta = 3$ and 11, exhibiting distinct surface flow patterns. The short-wavelength instability ($\beta = 11$) is the stronger of the two, producing the wall-shear distribution that portrays a 3-D flow pattern.

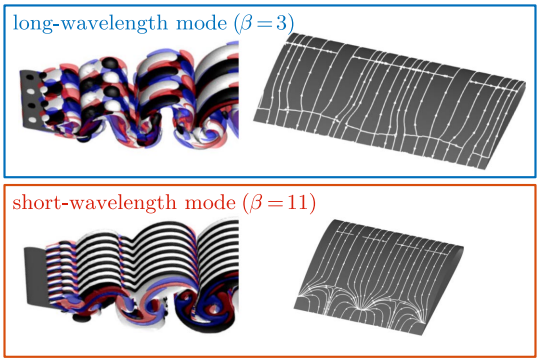

Fig. 11 Floquet analysis of the periodic flow over a NACA 4415 airfoil at $Re = 500$ and $\alpha = 20$ deg revealed two 3-D instability modes at $\beta = 3$ (top) and 11 (bottom) [140]; modal structures and surface streamlines are shown for each mode. (Reprinted with permission from Cambridge University Press.)

C. Flow Control

1. *Separation Control Using the Resolvent Analysis*

An airfoil at a high angle of attack or in an unsteady maneuver can experience stall resulting from flow separation over the suction surface [120,141–144]. To address this issue, the development of a separation-control technique to suppress flow separation has been the focus of many studies [120,145–147]. The study conducted by Yeh and Taira [43] considered the use of the resolvent analysis to guide an active separation control with periodic forcing. The analysis was conducted about the turbulent mean flows obtained from the baseline (uncontrolled) simulation to determine the optimal actuation frequencies and wave numbers to suppress separation. As a precursor to the resolvent analysis, a global stability analysis was conducted, which revealed an asymptotic instability of their base flows. To extend the resolvent analysis to the unstable base flows, a finite time (discounted) analysis [148] was applied by selecting a complex frequency $\omega = \omega_r - i\alpha$ in the resolvent operator $H(\omega) = [i\omega I - L_{\bar{q}}]^{-1}$. The real-valued discounting parameter α was chosen to be higher than the dominant unstable modal growth rate of $L_{\bar{q}}$ from the companion global stability analysis, such that the energy amplification in the input/output analysis is examined over a shorter timescale than that of the dominant instability.

Flow separation can be suppressed by the entrainment of freestream momentum over the suction surface, which can be achieved by enhancing the momentum mixing. As such, Yeh and Taira [43] proposed a modal mixing metric $M(\beta,\omega) \equiv \int_\Omega [\sigma^2(\hat{R}_x^2 + \hat{R}_y^2 + \hat{R}_z^2)^{1/2}]_{\beta,\omega} w(\boldsymbol{x})\, d\boldsymbol{x}$ that incorporates the response modal Reynolds stresses $\hat{R}$ and the associated gain σ from the resolvent analysis, with the spatial weight function $w(\boldsymbol{x})$ that encompasses the shear-layer region over the suction surface. This scalar metric M is a function of the spanwise wave number β and frequency ω, and quantifies the momentum mixing that takes place over the separation bubble. With enhanced freestream entrainment, the scalar function $M(\beta,\omega)$ assesses the effectiveness of the choice (β,ω) in suppressing flow separation. Supported by the independent parametric study on open-loop controlled flows, the modal mixing metric $M(\beta,\omega)$ was found to predict the enhancement of aerodynamic performance over the actuation parameter space of β and ω. The agreement between $M(\beta,\omega)$ and the performance enhancement is presented in Fig. 12, in which two cases are highlighted by showing the resolvent modes and visualization of instantaneous flowfield. In Fig. 12a, high amplification and strong modal Reynolds stresses over the suction surface gave rise

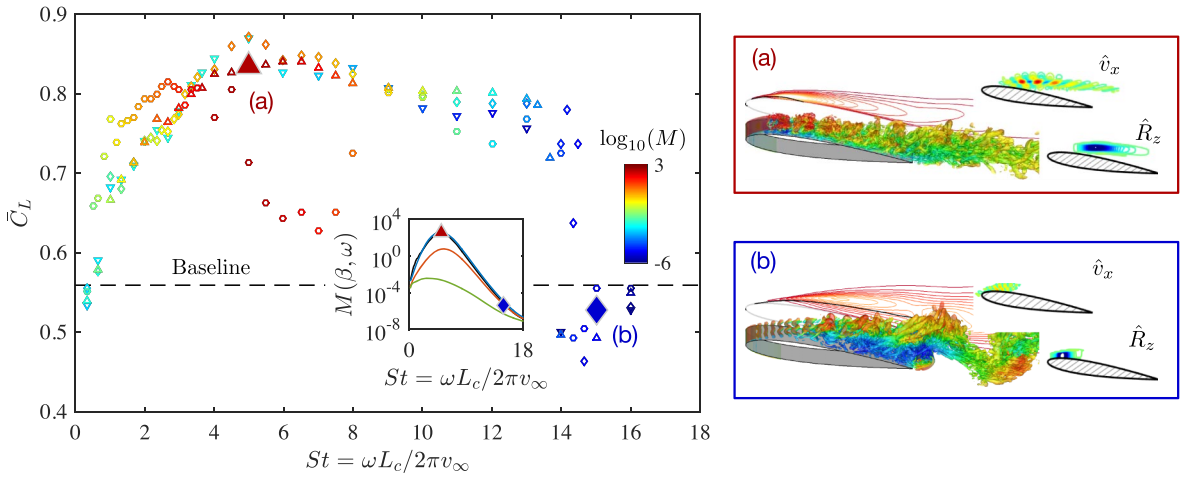

Fig. 12 Use of the resolvent analysis to develop separation control for an airfoil wake at $Re = 23{,}000$ [43]; control effectiveness is well predicted by the modal mixing function $M(\beta, \omega)$; a–b) visualizations are shown for the instantaneous flowfields and the resolvent response modes (streamwise velocity component) and the spanwise modal Reynolds stress $\hat{R}_z = Re(\hat{v}_x^* \hat{v}_y)$.

to the peak magnitude of the modal mixing metric $M(\beta, \omega)$. The companion large-eddy simulation (LES) confirmed a high level of momentum mixing induced by flow control using actuation with these parameters of (β, ω), which attached the flow and achieved enhancement in both lift and drag. In contrast, poor performance enhancement (Fig. 12b) with insufficient mixing provided by the small roll-up structure is also suggested by the resolvent response mode and low level of $M(\beta, \omega)$. This example of using a modal analysis provides quantitative assessments of the control effectiveness over a parameter space without the need for a computationally expensive LES parameter study.

2. *Attenuation of Wingtip Vortex*

Another important feature of an airfoil wake is the tip vortex. A finite span wing at an angle of attack creates a tip vortex due to the pressure difference between the suction and pressure surfaces. Because tip vortices have implications for efficiency loss, safety concerns, and wake unsteadiness, there have been a number of efforts to characterize the tip vortex [124,149,150]. Flow unsteadiness and instabilities around a wingtip have been studied with a modal analysis as well. In the experimental work of Edstrand et al. [126], a POD analysis of the wake on cross-stream planes [from particle image velocimetry (PIV) measurements at $Re = 530{,}000$ and $\alpha = 5$ deg] revealed modes associated with the so-called wandering phenomenon of the tip vortex. The modal structures from the POD were compared to the stability modes obtained for a Batchelor vortex model, exhibiting a great similarity. This observation suggests the wandering phenomenon to be closely related to the tip-vortex instability.

The prolonged presence of tip vortices is a safety hazard for aircraft operations. To address this issue, there have been efforts to attenuate the tip vortices with an active flow control. The traditional approach introduces perturbations from the wingtip in hopes of weakening the tip vortex [151,152]. In a recent study by Edstrand et al. [127], the wake behind the wingtip was computationally analyzed via a global stability analysis with a parabolized formulation incorporated in the streamwise direction ($Re = 1000$ and angle of attack of 5 deg). A similar approach was taken in an earlier study of the 3-D stability characteristics of an elliptic wing wake by He et al. [153]. In the detailed analysis of Edstrand et al. [127], they revealed two distinct types of instabilities, as visualized in Fig. 13. The dominant modes were found to possess structures that corotate with the tip vortex. They also found the subdominant fifth instability mode that emanates from the trailing edge with structures that counter-rotate with the tip vortex. Because past studies have revealed that counter-rotating instability modes can effectively attenuate vortices in free space, this finding suggested the forcing input to be introduced from the trailing edge to attenuate the tip vortex, instead of the wingtip. Using DNS, the tip vortex was found to be weakened effectively with the fifth-mode-based control setup, as shown by the circulation of the tip vortex in Fig. 13. To ensure that the control technique does indeed trigger the counter-rotating instability, DMD was also used to assess the controlled flow, for which the expected counter-rotating perturbation was observed. This study shows that a detailed stability

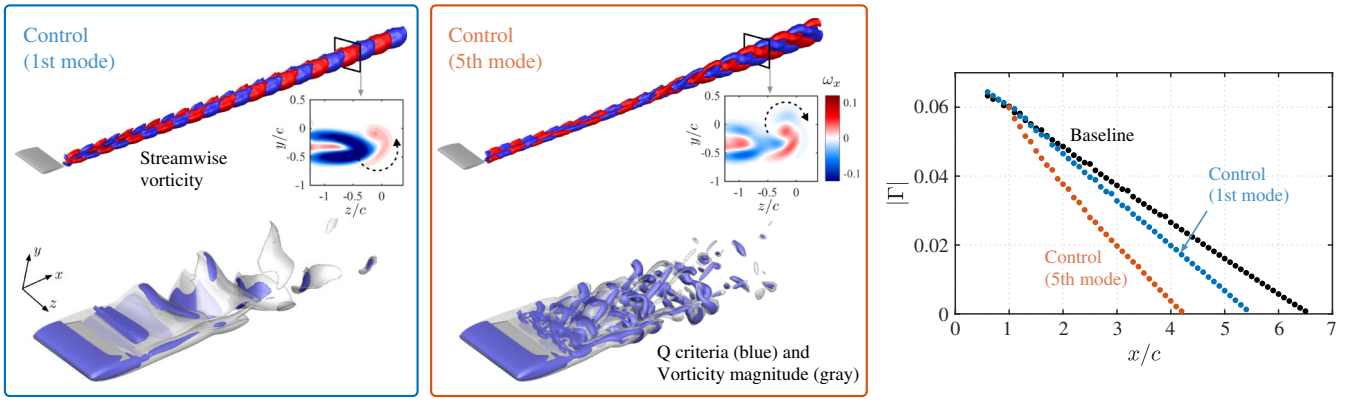

Fig. 13 First and fifth instability modes visualized (top); the modal profiles are used to introduce perturbations near the trailing edge to modify the wake and attenuate the tip vortex (bottom); circulation of the tip vortex is compared (right) to assess the effectiveness of active flow control. (Compiled with permission from Edstrand et al. [127]; reprinted with permission from Cambridge University Press.)

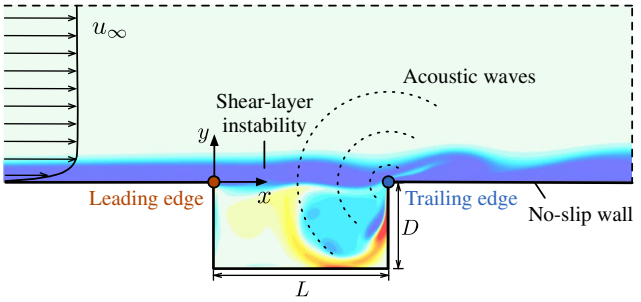

Fig. 14 Schematic of open-cavity flow with spanwise vorticity in the background.

analysis can be used to design an effective control technique, and identify the appropriate placement of the forcing input.

V. Cavity Flows

Flows over rectangular cavities serve as fundamental models for flows over landing-gear wells and stores on aircraft [154]. In an open-cavity flow, a shear layer forms from the leading edge and amplifies disturbances through the Kelvin–Helmholtz instability, which leads to the formation of large vortical structures that impinge on the cavity aft wall. Large pressure fluctuations and acoustic waves are generated from the impingement, which perturb the upstream shear layer. This overall process forms a self-sustained natural feedback loop in open-cavity flows, as shown in Fig. 14. Resonant tones are generated from this process, which are known as the *Rossiter modes* [155]. Based on a large collection of experimental data, Rossiter derived a semi-empirical formula to predict the resonant frequencies. As the original formula only considers the influence of the two important parameters of the freestream Mach number M_∞ and cavity aspect ratio L/D, extensive experimental and numerical studies have followed to examine the influence of other parameters, including the Reynolds number and boundary-layer thickness [156–158].

The spatial structures that correspond to the dominant Rossiter frequencies as well as the coherent structures that arise from other types of instabilities or physics can be revealed by modal-analysis techniques. This section considers the applications of modal-analysis techniques on rectangular open-cavity flows. We further discuss ways to design flow-control techniques to suppress flow oscillations based on insights from these modal analyses. In what follows, we will focus on spanwise-periodic rectangular cavity flows, unless otherwise noted.

A. POD and DMD Analyses

Given a collection of snapshots of open-cavity flows from experiments or simulations, we can perform a data-based analysis with POD and DMD. As discussed in Sec. II on cylinder flow, performing POD and DMD analyses requires a proper collection of snapshots to capture specific modes. For a laminar cavity flow, the appropriate number of snapshots and length of time-series data can be estimated based on the fundamental Rossiter frequencies given by the semi-empirical formula. For a turbulent cavity flow, a large number of snapshots become necessary, as such flow possesses spectra with a broader frequency content.

A POD analysis captures modes with large unsteady fluctuations. An example of applying a POD analysis of a turbulent flow over a cavity of $L/D = 6$ for $0.19 \leq M_\infty \leq 0.73$ from experiments has been briefly presented in our previous overview paper [1] (see sec. III.B.2 and Murray et al. [157]). Snapshots were collected using PIV from high-speed flows. For compressible cavity flows, the spatial structures of the most energetic POD modes reside in the shear-layer region, showing the spatially growing nature of the modes toward the cavity trailing edge [157], which remain similar regardless of the freestream Mach number. The POD analysis offers a framework to extract dominant energetic structures, and serves as a foundation for systematic comparison over a range of operating conditions.

We can alternatively use the DMD analysis to extract dynamically important modes. If the flowfield from a linearized Navier–Stokes solver is considered, the DMD analysis can return the global stability modes, as performed for a linearized flow over a cavity of $L/D = 1$ at $Re = 4500$ by Schmid [6]. Such an analysis identifies the Kelvin–Helmholtz instabilities in the shear layer that cause flow oscillations. As shown in Fig. 15, the branch of DMD eigenspectrum containing unstable modes ($\lambda_r > 0$) corresponds to shear-layer instabilities, as their modal structures are concentrated in the shear-layer region spanning the length of the cavity. Instead of performing DMD on linear snapshots, regressions can also be applied to extract global instability modes. Brès and Colonius [159] conducted extensive linearized simulations and extracted 3-D instabilities of a compressible open-cavity flow using a regression approach.

B. Global Stability and Resolvent Analyses

Because an open-cavity flow is globally affected by the Rossiter modes, a biglobal stability analysis is widely used to study the perturbation dynamics about a given 2-D base flow. Here, let us consider the perturbations to be spanwise periodic with a spanwise wave number of β (normalized by cavity depth). The biglobal stability analysis assumes a homogeneous direction, which we take to be periodic for the present discussion. If sidewall effects or any other 3-D factors need to be considered, a triglobal stability analysis can be adopted. For the biglobal stability analysis with $\beta = 0$, 2-D eigenmodes can be found, which are closely related to the well-known Rossiter modes, and 3-D instabilities can be determined by choosing $\beta > 0$ [160–163].

The insights gained from the modal analysis can be leveraged to develop active flow-control techniques to reduce the high-amplitude fluctuations in cavity flows. Sun et al. [163] performed a biglobal stability analysis of laminar compressible flows over a long cavity of $L/D = 6$ and $Re_D = 502$ to derive physics-based techniques for the attenuation of unsteady oscillations. In their study, they examined the influence of Mach number M_∞ and spanwise wavelength λ/D on the 3-D instability properties. It was found that the frequencies associated with 3-D instabilities ($\beta > 0$) are one order of magnitude lower than those of the 2-D shear-layer instabilities. The characteristics of the leading eigenmodes over a range of M_∞ and λ/D can be found, as shown in Fig. 16a. An increase in Mach number stabilizes the 3-D leading eigenmodes. Furthermore, they noticed that the overall trend of growth rate $\omega_i D/u_\infty$ remained similar over the range of Mach numbers considered. This suggests that flow-control strategies we design based on 3-D instabilities may work

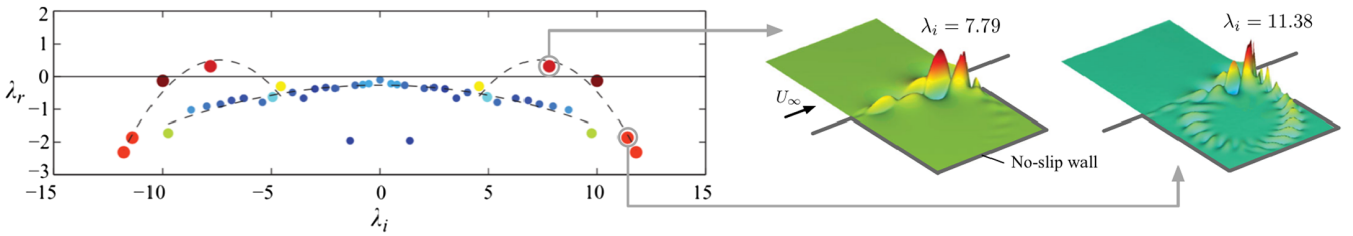

Fig. 15 DMD eigenspectrum (λ_i, frequency; λ_r, growth/decay rate) for incompressible flow over cavity of $L/D = 1$ and $Re = 4500$ (figure adapted from [6]); inserted are streamwise velocity of dynamic modes; the size and color of eigenvalues represent the coherence measurement of each mode with respect to its structure size and energetic level. (Reprinted with permission from Cambridge University Press.)

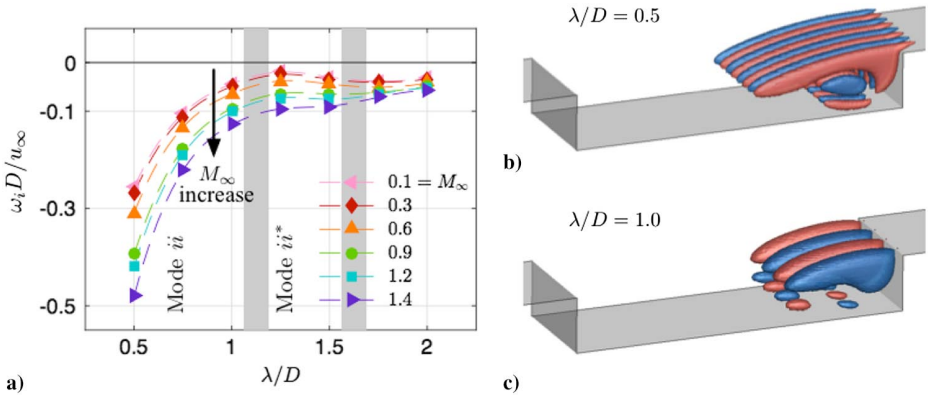

Fig. 16 Biglobal stability results of compressible flows over cavity with $L/D = 6$ at $Re_D = 502$ and $M_\infty \in [0.1,1.4]$ (figure adapted from [163]); a) growth rate $\omega_i D/u_\infty$ vs spanwise wavelength $\lambda/D = 2\pi/\beta$; b–c) spanwise velocity isosurfaces of the leading eigenmodes at $M_\infty = 0.9$. (Reprinted with permission from Cambridge University Press.)

across such a range of Mach numbers. Shown in Figs. 16b and 16c are the isosurfaces of the leading eigenmodes with $\lambda/D = 0.5$ and 1. The 3-D eigenmodes stem from centrifugal instabilities and are mainly concentrated in the rear part of the cavity where the recirculation zone resides. We can envision triggering the 3-D instabilities to potentially remove KE from the shear layer, and transfer them into the cavity. Taking advantage of the 3-D flow instabilities is an efficient way to modify the flowfield, as we shall see in Sec. V.C.

The resolvent analysis is capable of examining flow frequency response to harmonic forcing with respect to its base state. The optimal forcing and response modes can be identified according to their amplification gain σ obtained by performing singular-value decomposition of a resolvent operator $[i\omega I - L_{\bar{q}}]^{-1}$. Shown in Fig. 17 are some results of the resolvent analysis of a laminar flow over a cavity of $L/D = 6$ at $Re = 502$ and $M_\infty = 0.6$ by Liu et al. [164]. By sweeping over a normalized frequency $St_D = \omega D/(2\pi u_\infty)$, a maximum gain appears around $St_D \approx 0.15$ (Fig. 17a), which is not directly linked to the frequency of the leading eigenmode from the global stability analysis. This was also observed by Qadri and Schmid [165], suggesting that the difference in the peaks is caused by the nonnormality of the linear operator. As seen in Figs. 17b and 17c, the optimal forcing and response modes show their presence around the cavity leading edge and trailing edge, respectively. We found that the spatial structures of both modes emerge in the shear-layer region, which signifies the importance of shear-layer physics in an open-cavity flow.

Thus far, the discussions on cavity flows have assumed spanwise periodicity. However, the presence of sidewalls is known to influence the global characteristics of the cavity flows [158,166–168]. The sidewall effects on open-cavity flows can be considered by performing full 3-D simulations and a triglobal analysis without any Fourier expansions in the spanwise direction [169].

C. Flow Control

Insights from a modal analysis can serve as a useful tool for the design of active flow-control techniques. Here, we highlight some of the recent efforts on performing open- and closed-loop control of cavity flows based on modal analysis. To suppress the hydrodynamic and pressure oscillations in cavity flows with an open-loop control, actuators can be placed along the leading edge of the cavity in a 2-D or 3-D arrangement. Two-dimensional control setups (spanwise invariant setting) have been examined experimentally [170–172], but the simultaneous suppression of all resonant tones remains a challenge. On the other hand, 3-D actuation (spanwise varying) has been found to be effective in reducing amplitudes across all resonant tones [168,173–175].

A modal analysis can help select the appropriate spanwise spacing between actuators placed along the leading edge in a 3-D setup. That is, the preferred spanwise wavelength λ (or wave number $\beta = 2\pi/\lambda$) can be sought through a biglobal stability or resolvent analysis. For example, Sun et al. [168] have used the insights from a biglobal stability analysis to control a turbulent flow over a spanwise periodic cavity of $L/D = 6$. The goal of their work was to stimulate the emergence of 3-D modes to remove KE from the dominant 2-D shear-layer modes that are responsible for the large-amplitude fluctuations. The baseline and controlled flows from their study for $Re_D = 10^4$ and $M_\infty = 0.6$ are shown in Fig. 18. The controlled flow uses a steady-jet actuation with a spanwise wave number that corresponds to the leading 3-D stability mode, as reported in Fig. 16. The stability analysis was performed for a much lower $Re_D = 502$, whereas the insights from the modal analysis appear to span across Reynolds number and effectively modify the turbulent cavity flow. As visualized in Fig. 18 with the Q criterion [176], spanwise coherent structures appearing in the baseline flow (around $x/D \approx 2$) are inhibited in the controlled flow due to the 3-D streaks introduced by the steady blowing. By preventing the spanwise shear-layer rollups, a significant reduction in the levels of hydrodynamic and acoustic fluctuations is achieved, as seen from the rms of pressure displayed in subplots. The control strategy presented here has also shown its effectiveness in reducing pressure fluctuations for supersonic flows [177,178], as well as those for finite span cavities [168].

We can also use the spatial modes from the modal analysis to reduce the state dimension of a cavity flow and develop feedback

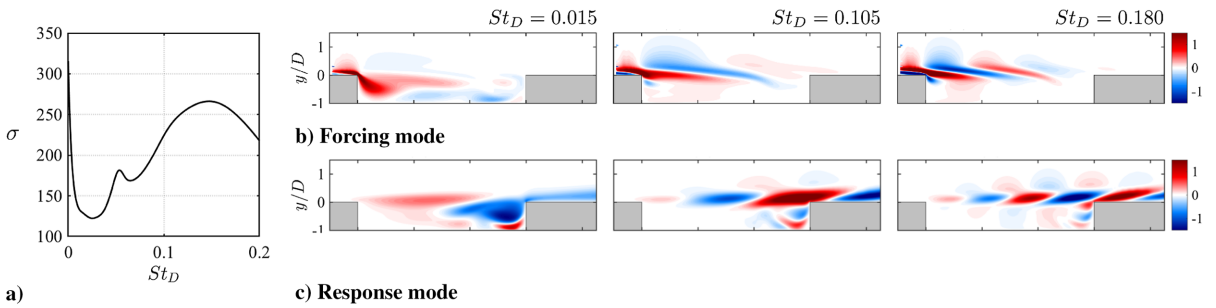

Fig. 17 Resolvent analysis of compressible cavity flow of $L/D = 6$, $Re_D = 502$, $M_\infty = 0.6$, and $\beta = 2$; a) optimal amplification gain, b) optimal forcing modes, and c) optimal response modes; contours of the streamwise velocity are visualized.

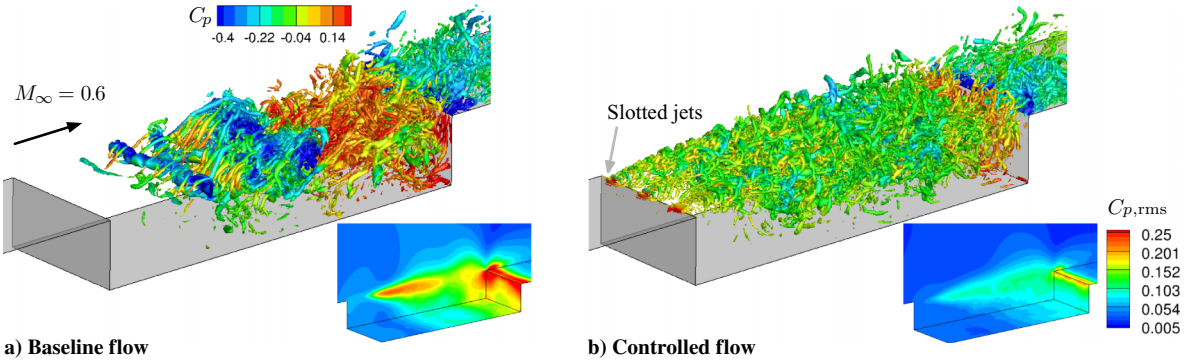

Fig. 18 Active control of turbulent flow over a cavity of $L/D = 6$ at $Re_D = 10^4$ and $M_\infty = 0.6$ using 3-D slotted jets along the leading edge (figure adapted from [168]); Q isosurface colored with the pressure coefficient C_p is visualized over the cavity; inserted plots show the pressure fluctuations.

(closed-loop) control strategies. An ROM of the cavity flow can be obtained via projecting the state dynamics onto an appropriate set of modes. In the work of Barbagallo et al. [179], the global, POD, and BPOD modes were considered to design a closed-loop control of an incompressible 2-D open-cavity flow at $Re_D = 7500$ to suppress the flow unsteadiness. An actuator and a sensor are placed on the walls and near the cavity leading and trailing edges, respectively. The actuator input was specified through wall-normal unsteady blowing/suction, whereas the output was taken to be the wall-normal shear stress integrated over the spanwise extent of the sensor.

Barbagallo et al. [179] computed the global instability modes by solving the eigenvalue problems resulting from the linearized Navier–Stokes equations about the unstable steady state. The POD and BPOD modes were determined by using the snapshots of the impulse response of the flowfield. Once the modes were obtained, the POD and BPOD modes were arranged in the order of the energy content and Hankel singular values, respectively, and the global modes were ordered according to their growth rates. The findings showed that the POD and BPOD modes performed well in modeling and suppressing the cavity-flow oscillations. The POD modes appear to exhibit robustness in the model, whereas the BPOD-based model is able to use far fewer modes compared to the POD-based model to develop a feedback-control law, because the BPOD modes effectively balance the controllability and observability of the system. The ROM constructed from global modes, on the other hand, overemphasized the contributions from the highly damped modes to the input/output behavior.

D. Landing-Gear Well

We close this section on cavity flows by presenting an application of modal analysis to a turbulent flow over a landing-gear well of a commercial aircraft model by Ricciardi et al. [180]. The turbulent flowfield obtained from a delayed detached-eddy simulation and the extracted dominant POD modes are shown in Fig. 19. In this analysis, they identified the velocity POD modes [181] that correlate with vortical structures responsible for generating the acoustic tones. Although the turbulent flow over the landing-gear well is highly complex, the shear-layer modes appear clearly, sharing a great similarity with those from fundamental cavity flows. This example highlights the importance of basic insights gained from a basis modal analysis being beneficial for practical applications.

VI. Outlook

In this review, we have explored a number of modal-analysis applications for fluid flows, ranging from simple, canonical flows to highly complex, real-world engineering configurations. One key takeaway is that each flow has its own unique blend of challenges, including high-dimensionality, nonlinearity, multiscale phenomena, complex geometry, and nonnormality. In this outlook, we discuss challenges and limitations of existing methods, as well as emerging techniques in machine learning and data science to address these challenges for reduced-order modeling and control. We summarize several important avenues of ongoing research that are likely to have a significant impact on modal analysis in fluids.

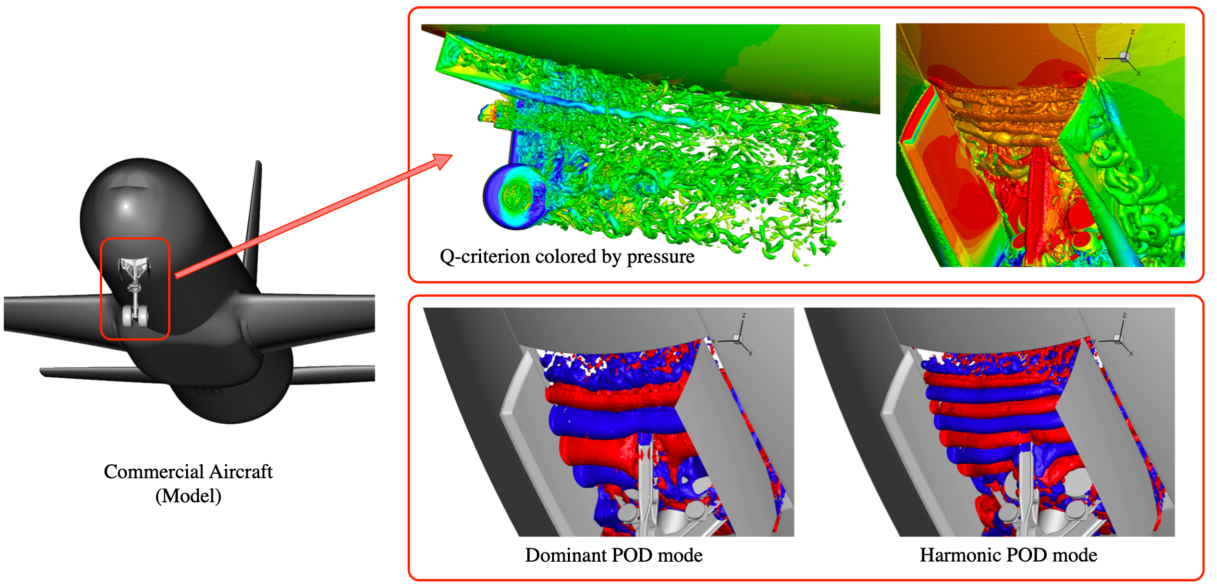

Fig. 19 Turbulent flow over a model landing-gear well of a commercial aircraft (top); transverse velocity POD mode captures the structures responsible for noise generation (bottom). (Adapted from [180] and reprinted with permission from the AIAA.)

A. Beyond Linear Superposition and Separation of Variables

Most of the modal-extraction techniques discussed earlier have been fundamentally linear, relying on superposition. For example, the POD and DMD modal bases both approximate the flowfield in terms of a linear combination of these modes. However, we know that many flows evolve on a low-dimensional manifold [56], rather than a low-dimensional linear subspace. Thus, there is a potential to obtain more accurate and efficient ROMs with nonlinear dimensionality reduction techniques. There are a number of effective techniques, for example, based on locally linear embedding [182,183] and Grassmannian manifolds [184,185]. In machine learning, the autoencoder is a neural network that embeds high-dimensional data into a low-dimensional latent space, followed by a decoder network that lifts back to the ambient high-dimensional space. Linear autoencoders have been shown to identify reduced subspaces similar to those found with POD, and they may be generalized to develop nonlinear analogues of POD [186,187]. Moreover, it has been shown that sufficiently large networks can represent arbitrarily complex input/output functions [188]. For this reason, deep network architectures [189–191] are becoming increasingly useful for modeling fluids and dynamic systems more generally. For example, deep learning has been recently used to identify nonlinear embeddings, in which the dynamics are linear [192–197], inspired by the Koopman theory [10,198,199]. However, note that deep learning requires extremely large volumes of training data, and resulting models are generally only useful for interpolation.

Snapshot-based dimensionality reduction methods that use the singular-value decomposition, such as POD and DMD, are fundamentally based on a space-time separation of variables. This can be seen clearly from the POD expansion in Eq. (3). However, many problems in fluid mechanics involve traveling wave phenomena that are not well modeled by separation of variables. Simple symmetry transformations of a coherent structure, such as translations and rotations, will result in a large number of POD modes [200]. Moving away from this space-time separation of variables is one of the most important open challenges in modal analysis, with the potential to improve how we describe and model convecting coherent structures.

B. Sparse and Randomized Algorithms

Dimensionality reduction and sparse algorithms are synergistic in that underlying low-dimensional representations facilitate sparse measurements [201,202] and fast randomized computations [203]. Compressed sensing has already been leveraged for compact representations of wall-bounded turbulence [204] and for POD-based flow reconstruction [205]. If only classification or detection is required, reconstruction can be circumvented and the measurements can become orders-of-magnitude sparser [206–208]. Decreasing the amount of data to train and execute a model is important when a fast decision is required, as in control.

Low-dimensional structure in data also facilitates acceleration of computations via randomized linear algebra [203,209]. If a matrix has a low-rank structure, there are efficient matrix-decomposition algorithms based on random sampling that can be adopted. The basic idea is that, if a large matrix has a low-dimensional structure, then with high probability this structure will be preserved after randomly projecting the columns or rows onto a low-dimensional subspace, facilitating efficient computations. These so-called randomized numerical methods have the potential to transform computational linear algebra, providing accurate matrix decompositions at a fraction of the cost of deterministic methods. For example, randomized linear algebra may be used to efficiently compute the singular-value decomposition. Randomized POD [210,211], randomized DMD [40,212,213], and randomized resolvent analysis [94,214] have also been developed based on the same principles.

C. Machine Learning for ROMs and Closures

Beyond a detailed analysis and characterization of fluid flows, one of the overarching goals of modal analysis is the construction of predictive models that may be used for design, optimization, estimation, and control. One of the primary challenges for effective flow control is the computational complexity and latency associated with making a control decision, which may introduce unacceptable time delays and destroy robust control performance [68]. Fully resolved simulations of multiscale flow phenomena are generally too slow for real-time feedback control. Thus, significant effort has gone into developing ROMs, with the goal of accurately and efficiently reproducing only the most relevant flow mechanisms [74,215]. A classical approach that involves Galerkin projection of the governing Navier–Stokes equations onto an orthogonal basis, such as Fourier or POD modes, results in a system of ODEs for the mode coefficients. Alternative data-driven approaches may be used to develop ROMs via system identification. In both cases, machine learning techniques are emerging to improve the modal basis and models. For instance, deep feedforward neural networks can be combined with POD-based modal-analysis techniques to develop accurate ROMs even for high-Reynolds-number flows [216].

Increasingly, machine learning is being used directly to build ROMs of physical systems from data. These approaches may be broadly categorized into methods that identify self-contained models [65–66,217–224] and methods that develop closures for existing coarse-grained models, such as POD–Galerkin [225], Reynolds-averaged Navier–Stokes [226–231], and LES [232]; for an excellent review of data-driven closure models, see [233]. It is also important to distinguish what types of input data are required to construct a ROM, including resolution in space and time; volume and quality of data; and whether or not experimentally inaccessible information, such as from an adjoint simulation, is required.

Because fluid-flow modeling is central to many applications in health, security, and transportation, it is often essential that models be interpretable. It is no surprise that these are among the leading challenges in machine learning and artificial intelligence research. The data-driven modeling of fluid flows is a rapidly growing field. Thus, we provide a high-level summary of some representative examples.

1. *Dynamic System Models*

There are several approaches for the modeling of time-series data that have been applied to fluid-flow systems. Neural networks are often used for nonlinear system identification, as in the nonlinear autoregressive moving average with exogenous input [217,220]. Long short-term memory networks, which have been widely applied for speech recognition, are now being used to model chaotic dynamic systems [221,222]. Deep learning is also being broadly used to model systems in physics [223,224]. Kernel methods have been employed to enrich the space of measurement functions used to approximate the Koopman operator via the extended DMD [218,219]. However, neural networks and kernel methods typically result in black-box models that may be prone to overfitting, unless care is taken to cross-validate the results. In modeling dynamic systems, the principle of parsimony states that a model should have the lowest complexity possible, while still faithfully representing the observed phenomena. That is, the balance between model complexity and model misfit is of central importance. This balance is helpful for preventing overfitting and promoting models that are interpretable—because there are only a few terms in the model that may be connected to physical interactions—and generalizable [64]. The SINDy method identifies the fewest terms required to model time-series data with a differential equation, and has recently been applied to model various fluid flows [65,66,234]. By building models directly on physically intrinsic quantities, such as lift and drag measurements, these models bypass the well-known challenges of projection-based methods of continuous mode deformation associated with changing geometry and flow conditions [66]. Similar approaches have also been considered from the standpoint of prediction-error and subspace-identification techniques for parameter-varying models [235], albeit without the advantage of model interpretability. It is also possible to combine modal analysis with the theory of networked dynamic systems [60,236–242]. Network-based approaches have been used in several novel flow applications [240], including to obtain cluster ROMs of complex flows [238,239], to model 2-D isotropic

turbulence [241], to model and control wake flows [60], and for community detection in wake flows [242]. Finally, many of the aforementioned methods, including DMD with control [243], extended DMD [244], streaming DMD [42,245,246], and SINDy, have been used in conjunction with model predictive control to tame complex dynamic systems and fluid flows [247–250].

2. *Closure Models and Stabilization*

Many classical reduced-order modeling approaches involve truncating the modal basis to only include large, dominant, energetic coherent structures, neglecting the detailed modeling of fine-scale structures. However, even if the truncated modes do not contain a significant portion of the energy, they can still play a significant role in the dynamics and stability of the ROM [251]. A variety of strategies have been developed that compute appropriate projections to ensure stability. These efforts include energy-based inner products [252,253], symmetry transformations [254], and the least-squares Petrov–Galerkin (LSPG) approach [255]. From a practical standpoint, the LSPG method has to be employed with hyper-reduction, which will be discussed in the next section, because without hyper-reduction, the computational cost of LSPG may be higher than that of the original full-order model. From a closure viewpoint, inaccuracies, which can lead to instabilities, are considered to result from the impact of the unresolved physics on the resolved modes. Indeed, the error evolution is related to the closure terms, which is the target of subgrid-scale modeling in LESs. Research has examined the construction of mixing length [54], Smagorinsky-type [251,256–258], and variational multiscale (VMS) closures [251,259,260]. Another approach that displays similarities to the VMS method is the Mori–Zwanzig (MZ) formalism [261–266]. In VMS- and MZ-based approaches, the state variables are decomposed into a resolved set and an unresolved set. The impact of the unresolved scales on the resolved scales is then modeled. Parish and Duraisamy [267] represented and modeled unresolved physics in the form of a memory integral that depends on the temporal history of the coarse-scale variables. This approach presents a unified view of VMS closures and Petrov–Galerkin stabilization.

3. *Hyper-Reduction*

Even though the ROM equations are in terms of a reduced state of dimension r, the projected dynamics require evaluation of the high-dimensional nonlinear dynamics, which are of dimension $n \gg r$. This limits the utility of ROMs of nonlinear systems, as the online cost can scale as $\mathcal{O}(n)$. Thus, beyond reducing the order of a model, acceleration (or alternately hyper-reduction or sparse sampling) techniques will be required to improve the efficiency of a ROM. The gappy POD method provides the ability to sparsely sample a system in $\mathcal{O}(r)$ locations, and still evaluate the POD and terms in the Galerkin projection [268,269]. In addition, there are reduced-basis methods for partial differential equations [270] and the associated discrete empirical interpolation method [271–273], which approximates nonlinear terms by evaluating the nonlinearity at a few points. This approach is also prevalent in high-performance computing [255,274–276], and may also impact flow control.

VII. Conclusions

As a sequel to the previous introductory overview paper on modal analysis [1], this document surveyed applications of modal-analysis techniques with the hope to serve as a go-to guide for readers seeking insights on how modal-analysis techniques can help analyze different types of flows. With such point in mind, the current paper focused on presenting applications of modal-analysis techniques to study, model, and control canonical aerodynamic flows. To illustrate how modal-analysis techniques can provide physical insights in a complementary manner, four fundamental examples of cylinder wakes, wall-bounded flows, airfoil wakes, and cavity flows have been selected. A good portion of the examples considered in this paper considered the applications of modal analysis for developing effective active flow-control strategies. Although this paper attempted to cover a range of topics, it is by no means comprehensive in nature. Readers with elevated levels of interests are invited to delve into the references for details.

Toward the end of this paper, some brief discussions on the outlook for modal-analysis techniques were also offered, in light of rapid developments in data science. As the emergence of many refreshing data-inspired concepts is seen, fluid mechanicians are in an exciting era to incorporate these ideas and extend modal-analysis techniques. In fact, there are ongoing developments in handling large data sets and constructing sparse interpretable models. It is believed that such efforts can enable the analysis of high-dimensional fluid flows with complex dynamics. The implementation of these approaches is facilitated with the enhancement in the available computational resources. It is hoped that this overview paper, along with the first overview paper, serves as a valuable educational tool for engineers and scientists interested in performing modal analysis of aerodynamic flows.

Acknowledgments

This paper was one of the major outcomes from the AIAA Discussion Group (Fluid Dynamics Technical Committee) entitled "Modal Decomposition of Aerodynamic Flows" organized by Douglas Smith, Kunihiko Taira, Maziar Hemati, and Karthik Duraisamy. The authors thank the fruitful discussions with the members of the discussion group, and greatly acknowledge the generous support from the following agencies: Air Force Office of Scientific Research, Army Research Office, National Science Foundation, Office of Naval Research, and Defense Advanced Research Projects Agency. Lastly, the authors sincerely thank the Editor-in-Chief, Alexander Smits, and Associate Editor, Peyman Givi, of the *AIAA Journal* for supporting the overall effort to make this special section on modal analysis possible.

References

[1] Taira, K., Brunton, S. L., Dawson, S., Rowley, C. W., Colonius, T., McKeon, B. J., Schmidt, O. T., Gordeyev, S., Theofilis, V., and Ukeiley, L. S., "Modal Analysis of Fluid Flows: An Overview," *AIAA Journal*, Vol. 55, No. 12, 2017, pp. 4013–4041.

[2] Holmes, P., Lumley, J. L., Berkooz, G., and Rowley, C. W., *Turbulence, Coherent Structures, Dynamical Systems and Symmetry*, 2nd ed., Cambridge Univ. Press, Cambridge, 2012.

[3] Berkooz, G., Holmes, P., and Lumley, J. L., "The Proper Orthogonal Decomposition in the Analysis of Turbulent Flows," *Annual Review of Fluid Mechanics*, Vol. 25, No. 1, 1993, pp. 539–575.

[4] Rowley, C. W., "Model Reduction for Fluids Using Balanced Proper Orthogonal Decomposition," *International Journal of Bifurcation and Chaos in Applied Sciences and Engineering*, Vol. 15, No. 3, 2005, pp. 997–1013.

[5] Ilak, M., and Rowley, C. W., "Modeling of Transitional Channel Flow Using Balanced Proper Orthogonal Decomposition," *Physics of Fluids*, Vol. 20, No. 3, 2008, Paper 034103.

[6] Schmid, P. J., "Dynamic Mode Decomposition of Numerical and Experimental Data," *Journal of Fluid Mechanics*, Vol. 656, Nov. 2010, pp. 5–28.

[7] Rowley, C. W., Mezić, I., Bagheri, S., and Henningson, D. S., "Spectral Analysis of Nonlinear Flows," *Journal of Fluid Mechanics*, Vol. 641, Dec. 2009, pp. 115–127.

[8] Tu, J. H., Rowley, C. W., Luchtenburg, D. M., Brunton, S. L., and Kutz, J. N., "On Dynamic Mode Decomposition: Theory and Applications," *Journal of Computational and Nonlinear Dynamics*, Vol. 1, No. 2, 2014, pp. 391–421.

[9] Kutz, J. N., Brunton, S. L., Brunton, B. W., and Proctor, J. L., *Dynamic Mode Decomposition: Data-Driven Modeling of Complex Systems*, Soc. for Industrial and Applied Mathematics, Philadelphia, 2016.

[10] Mezić, I., "Analysis of Fluid Flows via Spectral Properties of the Koopman Operator," *Annual Review of Fluid Mechanics*, Vol. 45, No. 1, 2013, pp. 357–378.

[11] Theofilis, V., "Advances in Global Linear Instability Analysis of Nonparallel and Three-Dimensional Flows," *Progress in Aerospace Sciences*, Vol. 39, No. 4, 2003, pp. 249–315.

[12] Theofilis, V., "Global Linear Instability," *Annual Review of Fluid Mechanics*, Vol. 43, No. 1, 2011, pp. 319–352.

[13] Trefethen, L. N., Trefethen, A. E., Reddy, S. C., and Driscoll, T. A., "Hydrodynamic Stability Without Eigenvalues," *Science*, Vol. 261, No. 5121, 1993, pp. 578–584.

[14] McKeon, B. J., Sharma, A. S., and Jacobi, I., "Experimental Manipulation of Wall Turbulence: A Systems Approach," *Physics of Fluids*, Vol. 25, No. 3, 2013, Paper 031301.

[15] Zdravkovich, M. M., *Flow Around Circular Cylinders, Vol. 1: Fundamentals*, Oxford Univ. Press, Oxford, 1997.

[16] Zdravkovich, M. M., *Flow Around Circular Cylinders, Vol 2: Applications*, Oxford Univ. Press, Oxford, 2003.

[17] von Kármán, T., "Über den Mechanismus des Widerstandes, den ein bewegter Körper in einer Flüsseigkeit afahrt," *Nachrichten von der Gesellschaft der Wissenschaften zu Göttingen, Mathematisch-Physikalische Klasse*, 1911, pp. 509–517.

[18] Roshko, A., "On the Development of Turbulent Wakes from Vortex Streets," NACA TR 1191, 1954.

[19] Coutanceau, M., and Bouard, R., "Experimental Determination of the Main Features of the Viscous Flow in the Wake of a Circular Cylinder in Uniform Translation, Part 1: Steady Flow," *Journal of Fluid Mechanics*, Vol. 79, No. 2, 1977, pp. 231–256.

[20] Coutanceau, M., and Bouard, R., "Experimental Determination of the Main Features of the Viscous Flow in the Wake of a Circular Cylinder in Uniform Translation, Part 2: Unsteady Flow," *Journal of Fluid Mechanics*, Vol. 79, No. 2, 1977, pp. 257–272.

[21] Williamson, C. H. K., and Roshko, A., "Vortex Formation in the Wake of an Oscillating Cylinder," *Journal of Fluids and Structures*, Vol. 2, No. 4, 1988, pp. 355–381.

[22] Williamson, C. H. K., "Vortex Dynamics in the Cylinder Wake," *Annual Review of Fluid Mechanics*, Vol. 28, No. 1, 1996, pp. 477–539.

[23] Roshko, A., "Experiments on the Flow Past a Circular Cylinder at Very High Reynolds Number," *Journal of Fluid Mechanics*, Vol. 10, No. 3, 1961, pp. 345–356.

[24] Noack, B. R., and Eckelmann, H., "A Global Stability Analysis of the Steady and Periodic Cylinder Wake," *Journal of Fluid Mechanics*, Vol. 270, July 1994, pp. 297–330.

[25] Giannetti, F., and Luchini, P., "Structural Sensitivity of the First Instability of the Cylinder Wake," *Journal of Fluid Mechanics*, Vol. 581, June 2007, pp. 167–197.

[26] Behara, S., and Mittal, S., "Wake Transition in Flow Past a Circular Cylinder," *Physics of Fluids*, Vol. 22, No. 11, 2010, Paper 114104.

[27] Canuto, D., and Taira, K., "Two-Dimensional Compressible Viscous Flow Around a Circular Cylinder," *Journal of Fluid Mechanics*, Vol. 785, Dec. 2015, pp. 349–371.

[28] Williamson, C., and Govardhan, R., "Vortex-Induced Vibrations," *Annual Review of Fluid Mechanics*, Vol. 36, No. 1, 2004, pp. 413–455.

[29] Sarpkaya, T., "A Critical Review of the Intrinsic Nature of Vortex-Induced Vibrations," *Journal of Fluids and Structures*, Vol. 19, No. 4, 2004, pp. 389–447.

[30] Tokumaru, P. T., and Dimotakis, P. E., "Rotary Oscillation Control of a Cylinder Wake," *Journal of Fluid Mechanics*, Vol. 224, March 1991, pp. 77–90.

[31] Kim, J., and Choi, H., "Distributed Forcing of Flow over a Circular Cylinder," *Physics of Fluids*, Vol. 17, No. 3, 2005, Paper 033103.

[32] Munday, P. M., and Taira, K., "On the Lock-On of Vortex Shedding to Oscillatory Actuation Around a Circular Cylinder," *Physics of Fluids*, Vol. 25, No. 1, 2013, Paper 013601.

[33] Taira, K., and Nakao, H., "Phase-Response Analysis of Synchronization for Periodic Flows," *Journal of Fluid Mechanics*, Vol. 846, July 2018, p. R2.

[34] Taira, K., and Colonius, T., "The Immersed Boundary Method: A Projection Approach," *Journal of Computational Physics*, Vol. 225, No. 2, 2007, pp. 2118–2137.

[35] Colonius, T., and Taira, K., "A Fast Immersed Boundary Method Using a Nullspace Approach and Multi-Domain Far-Field Boundary Conditions," *Computer Methods in Applied Mechanics and Engineering*, Vol. 197, Nos. 25–28, 2008, pp. 2131–2146.

[36] Sirovich, L., "Turbulence and the Dynamics of Coherent Structures, Parts I-III," *Quarterly of Applied Mathematics*, Vol. 45, No. 3, 1987, pp. 561–590.

[37] Chen, K. K., Tu, J. H., and Rowley, C. W., "Variants of Dynamic Mode Decomposition: Boundary Condition, Koopman, and Fourier Analyses," *Journal of Nonlinear Science*, Vol. 22, No. 6, 2012, pp. 887–915.

[38] Bagheri, S., "Koopman-Mode Decomposition of the Cylinder Wake," *Journal of Fluid Mechanics*, Vol. 726, July 2013, pp. 596–623.

[39] Duke, D., Soria, J., and Honnery, D., "An Error Analysis of the Dynamic Mode Decomposition," *Experiments in Fluids*, Vol. 52, No. 2, 2012, pp. 529–542.

[40] Hemati, M. S., Rowley, C. W., Deem, E. A., and Cattafesta, L. N., "De-Biasing the Dynamic Mode Decomposition for Applied Koopman Spectral Analysis of Noisy Datasets," *Theoretical and Computational Fluid Dynamics*, Vol. 31, No. 4, 2017, pp. 349–368.

[41] Dawson, S. T. M., Hemati, M. S., Williams, M. O., and Rowley, C. W., "Characterizing and Correcting for the Effect of Sensor Noise in the Dynamic Mode Decomposition," *Experiments in Fluids*, Vol. 57, No. 3, 2016, pp. 1–19.

[42] Hemati, M. S., Deem, E. A., Williams, M. O., Rowley, C. W., and Cattafesta, L. N., "Improving Separation Control with Noise-Robust Variants of Dynamic Mode Decomposition," AIAA Paper 2016-1103, 2016.

[43] Yeh, C.-A., and Taira, K., "Resolvent-Analysis-Based Design of Airfoil Separation Control," *Journal of Fluid Mechanics*, Vol. 867, May 2019, pp. 572–610.

[44] Taneda, S., "Experimental Investigation of the Wakes Behind Cylinders and Plates at Low Reynolds Numbers," *Journal of the Physical Society of Japan*, Vol. 11, No. 3, 1956, pp. 302–307.

[45] Strykowski, P. J., and Sreenivasan, K. R., "On the Formation and Suppression of Vortex 'Shedding' at Low Reynolds Numbers," *Journal of Fluid Mechanics*, Vol. 218, Sept. 1990, pp. 71–107.

[46] Zebib, A., "Stability of Viscous Flow Past a Circular Cylinder," *Journal of Engineering Mathematics*, Vol. 21, No. 2, 1987, pp. 155–165.

[47] Jackson, C. P., "A Finite-Element Study of the Onset of Vortex Shedding in Flow Past Variously Shaped Bodies," *Journal of Fluid Mechanics*, Vol. 182, Sept. 1987, pp. 23–45.

[48] Abdessemed, N., Sharma, A. S., Sherwin, S. J., and Theofilis, V., "Transient Growth Analysis of the Flow Past Circular Cylinder," *Physics of Fluids*, Vol. 21, No. 4, 2009, Paper 044103.

[49] Sipp, D., and Lebedev, A., "Global Stability of Base and Mean Flows: A General Approach and Its Applications to Cylinder and Open Cavity Flows," *Journal of Fluid Mechanics*, Vol. 593, Dec. 2007, pp. 333–358.

[50] Provansal, M., Mathis, C., and Boyer, L., "Bénard-von Kármán Instability: Transient and Forced Regimes," *Journal of Fluid Mechanics*, Vol. 182, Sept. 1987, pp. 1–22.

[51] Williamson, C. H. K., "The Existence of Two Stages in the Transition to Three-Dimensionality of a Cylinder Wake," *Physics of Fluids*, Vol. 31, No. 11, 1988, pp. 3165–3168.

[52] Williamson, C. H. K., "Three-Dimensional Wake Transition," *Journal of Fluid Mechanics*, Vol. 328, Dec. 1996, pp. 345–407.

[53] Barkley, D., and Henderson, R. D., "Three-Dimensional Floquet Stability Analysis of the Wake of a Circular Cylinder," *Journal of Fluid Mechanics*, Vol. 322, Sept. 1996, pp. 215–241.

[54] Aubry, N., Holmes, P., Lumley, J. L., and Stone, E., "The Dynamics of Coherent Structures in the Wall Region of a Turbulent Boundary Layer," *Journal of Fluid Mechanics*, Vol. 192, July 1988, pp. 115–173.

[55] Noack, B. R., Morzynski, M., and Tadmor, G. (eds.), *Reduced-Order Modelling for Flow Control*, Springer, New York, 2011.

[56] Noack, B. R., Afanasiev, K., Morzynski, M., Tadmor, G., and Thiele, F., "A Hierarchy of Low-Dimensional Models for the Transient and Post-Transient Cylinder Wake," *Journal of Fluid Mechanics*, Vol. 497, Dec. 2003, pp. 335–363.

[57] Bergmann, M., Bruneau, C.-H., and Iollo, A., "Enablers for Robust POD Models," *Journal of Computational Physics*, Vol. 228, No. 2, 2009, pp. 516–538.

[58] Deane, A. E., Kevrekidis, I. G., Karniadakis, G. E., and Orszag, S. A., "Low-Dimensional Models for Complex Geometry Flows: Application to Grooved Channels and Circular Cylinders," *Physics of Fluids A: Fluid Dynamics*, Vol. 3, No. 10, 1991, pp. 2337–2354.

[59] Zhang, W., and Wei, M., "Model Order Reduction Using DMD Modes and Adjoint DMD Modes," AIAA Paper 2017-3482, 2017.

[60] Nair, A. G., Brunton, S. L., and Taira, K., "Networked-Oscillator-Based Modeling and Control of Unsteady Wake Flows," *Physical Review E*, Vol. 97, No. 6, 2018, Paper 063107.

[61] Balajewicz, M. J., Dowell, E. H., and Noack, B. R., "Low-Dimensional Modelling of High-Reynolds-Number Shear Flows Incorporating Constraints from the Navier–Stokes Equation," *Journal of Fluid Mechanics*, Vol. 729, Aug. 2013, pp. 285–308.

[62] Carlberg, K., Tuminaro, R., and Boggs, P., "Preserving Lagrangian Structure in Nonlinear Model Reduction with Application to Structural Dynamics," *SIAM Journal on Scientific Computing*, Vol. 37, No. 2, 2015, pp. B153–B184.

[63] Schlegel, M., and Noack, B. R., "On Long-Term Boundedness of Galerkin Models," *Journal of Fluid Mechanics*, Vol. 765, Feb. 2015, pp. 325–352.

[64] Brunton, S. L., Proctor, J. L., and Kutz, J. N., "Discovering Governing Equations from Data by Sparse Identification of Nonlinear Dynamical Systems," *Proceedings of the National Academy of Sciences*, Vol. 113, No. 15, 2016, pp. 3932–3937.

[65] Loiseau, J.-C., and Brunton, S. L., "Constrained Sparse Galerkin Regression," *Journal of Fluid Mechanics*, Vol. 838, March 2018, pp. 42–67.

[66] Loiseau, J.-C., Noack, B. R., and Brunton, S. L., "Sparse Reduced-Order Modeling: Sensor-Based Dynamics to Full-State Estimation," *Journal of Fluid Mechanics*, Vol. 844, June 2018, pp. 459–490.

[67] Brunton, S. L., Noack, B. R., and Koumoutsakos, P., "Machine Learning in Fluid Mechanics," *Annual Review of Fluid Mechanics*, 2020 (to appear).

[68] Brunton, S. L., and Noack, B. R., "Closed-Loop Turbulence Control: Progress and Challenges," *Applied Mechanics Reviews*, Vol. 67, No. 5, 2015, Paper 050801.

[69] Orszag, S. A., "Accurate Solution of the Orr–Sommerfeld Stability Equation," *Journal of Fluid Mechanics*, Vol. 50, Dec. 1971, pp. 689–703.

[70] Schmid, P. J., "Nonmodal Stability Theory," *Annual Review of Fluid Mechanics*, Vol. 39, No. 1, 2007, pp. 129–162.

[71] Schmid, P. J., and Henningson, D. S., *Stability and Transition in Shear Flows*, Springer, New York, 2001.

[72] Jovanović, M. R., and Bamieh, B., "Componentwise Energy Amplification in Channel Flows," *Journal of Fluid Mechanics*, Vol. 534, July 2005, pp. 145–183.

[73] Kim, J., and Bewley, T. R., "A Linear Systems Approach to Flow Control," *Annual Review of Fluid Mechanics*, Vol. 39, No. 1, 2007, pp. 383–417.

[74] Rowley, C. W., and Dawson, S. T. M., "Model Reduction for Flow Analysis and Control," *Annual Review of Fluid Mechanics*, Vol. 49, No. 1, 2017, pp. 387–417.

[75] Reddy, S. C., Schmid, P. J., and Henningson, D. S., "Pseudospectra of the Orr–Sommerfeld Equation," *SIAM Journal on Applied Mathematics*, Vol. 53, No. 1, 1993, pp. 15–47.

[76] Trefethen, L. N., and Embree, M., *Spectra and Pseudospectra*, Princeton Univ. Press, Princeton, NJ, 2005.

[77] Moore, B. C., "Principal Component Analysis in Linear Systems: Controllability, Observability, and Model Reduction," *IEEE Transactions on Automatic Control*, Vol. 26, No. 1, 1981, pp. 17–32.

[78] Ahuja, S., and Rowley, C. W., "Feedback Control of Unstable Steady States of Flow Past a Flat Plate Using Reduced-Order Estimators," *Journal of Fluid Mechanics*, Vol. 645, Feb. 2010, pp. 447–478.

[79] Bhattacharjee, D., Hemati, M., Klose, B., and Jacobs, G., "Optimal Actuator Selection for Airfoil Separation Control," AIAA Paper 2018-3692, 2018.

[80] Yao, H., and Hemati, M., "Advances in Output Feedback Control of Transient Energy Growth in a Linearized Channel Flow," AIAA Paper 2019-0882, 2019.

[81] Martinelli, F., Quadrio, M., McKernan, J., and Whidborne, J., "Linear Feedback Control of Transient Energy Growth and Control Performance Limitations in Subcritical Plane Poiseuille Flow," *Physics of Fluids*, Vol. 23, No. 1, 2011, Paper 014103.

[82] Ilak, M., and Rowley, C., "Feedback Control of Transitional Channel Flow Using Balanced Proper Orthogonal Decomposition," AIAA Paper 2008-4230, 2008.

[83] Kalur, A., and Hemati, M., "Reduced-Order Models for Feedback Control of Transient Energy Growth," AIAA Paper 2018-3690, 2018.

[84] Kalur, A., and Hemati, M., "Control-Oriented Model Reduction for Minimizing Transient Energy Growth in Shear Flows," *AIAA Journal*, 2019.

[85] Hemati, M., and Yao, H., "Dynamic Mode Shaping for Fluid Flow Control: New Strategies for Transient Growth Suppression," AIAA Paper 2017-3160, 2017.

[86] Hemati, M., and Yao, H., "Performance Limitations of Observer-Based Feedback for Transient Energy Growth Suppression," *AIAA Journal*, Vol. 56, No. 6, 2018, pp. 2119–2123.

[87] Yao, H., and Hemati, M., "Revisiting the Separation Principle for Improved Transition Control," AIAA Paper 2018-3693, 2018.

[88] Jones, B. L., Heins, P. H., Kerrigan, E. C., Morrison, J. F., and Sharma, A. S., "Modelling for Robust Feedback Control of Fluid Flows," *Journal of Fluid Mechanics*, Vol. 769, April 2015, pp. 687–722.

[89] Reynolds, W., and Tiederman, W., "Stability of Turbulent Channel Flow, with Application to Malkus's Theory," *Journal of Fluid Mechanics*, Vol. 27, No. 2, 1967, pp. 253–272.

[90] del Álamo, J. C., and Jimenez, J., "Linear Energy Amplification in Turbulent Channels," *Journal of Fluid Mechanics*, Vol. 559, July 2006, pp. 205–213.

[91] Klebanoff, P. S., Tidstrom, K., and Sargent, L., "The Three-Dimensional Nature of Boundary-Layer Instability," *Journal of Fluid Mechanics*, Vol. 12, No. 1, 1962, pp. 1–34.

[92] Schoppa, W., and Hussain, F., "Coherent Structure Generation in Near-Wall Turbulence," *Journal of Fluid Mechanics*, Vol. 453, Feb. 2002, pp. 57–108.

[93] Sharma, A. S., and McKeon, B. J., "On Coherent Structure in Wall Turbulence," *Journal of Fluid Mechanics*, Vol. 728, Aug. 2013, pp. 196–238.

[94] Moarref, R., Sharma, A. S., Tropp, J. A., and McKeon, B. J., "Model-Based Scaling and Prediction of the Streamwise Energy Intensity in High-Reynolds Number Turbulent Channels," *Journal of Fluid Mechanics*, Vol. 734, Nov. 2013, pp. 275–316.

[95] Sharma, A. S., Moarref, R., and McKeon, B. J., "Scaling and Interaction of Self-Similar Modes in Models of High Reynolds Number Wall Turbulence," *Philosophical Transactions of the Royal Society A: Mathematical, Physical and Engineering Sciences*, Vol. 375, No. 2089, 2017, pp. 1–14.

[96] Farrell, B., and Ioannou, J., "Stochastic Forcing of the Linearized Navier–Stokes Equations," *Physics of Fluids*, Vol. 5, No. 11, 1993, pp. 2600–2609.

[97] Hwang, Y., and Cossu, C., "Linear Non-Normal Energy Amplification of Harmonic and Stochastic Forcing in the Turbulent Channel Flow," *Journal of Fluid Mechanics*, Vol. 664, Dec. 2010, pp. 51–73.

[98] McKeon, B. J., and Sharma, A. S., "A Critical Layer Model for Turbulent Pipe Flow," *Journal of Fluid Mechanics*, Vol. 658, Sept. 2010, pp. 336–382.

[99] Reddy, S. C., and Henningson, D. S., "Energy Growth in Viscous Channel Flows," *Journal of Fluid Mechanics*, Vol. 252, July 1993, pp. 209–238.

[100] Symon, S., Rosenberg, K., Dawson, S. T. M., and McKeon, B. J., "On Non-Normality and Classification of Amplification Mechanisms in Stability and Resolvent Analysis," *Physical Review Fluids*, Vol. 3, No. 5, 2018, Paper 053902.

[101] Luhar, M., Sharma, A. S., and McKeon, B. J., "A Framework for Studying the Effect of Compliant Surfaces on Wall Turbulence," *Journal of Fluid Mechanics*, Vol. 768, April 2015, pp. 415–441.

[102] Chavarin, A., and Luhar, M., "Resolvent Analysis for Turbulent Channel Flow with Riblets," *AIAA Journal*, 2019, pp. 1–11.

[103] Luhar, M., Sharma, A. S., and McKeon, B. J., "Opposition Control Within the Resolvent Analysis Framework," *Journal of Fluid Mechanics*, Vol. 749, June 2014, pp. 597–626.

[104] Towne, A., Schmidt, O. T., and Colonius, T., "Spectral Proper Orthogonal Decomposition and Its Relationship to Dynamic Mode Decomposition and Resolvent Analysis," *Journal of Fluid Mechanics*, Vol. 847, July 2018, pp. 821–867.

[105] Lumley, J. L., "The Structure of Inhomogeneous Turbulent Flows," *Proceedings of the International Colloquium on the Fine Scale Structure of the Atmosphere and Its Influence on Radio Wave Propagation*, edited by A. M. Yaglam, and V. I. Tatarsky, Nauka, Moscow, 1967.

[106] Lumley, J. L., "Coherent Structures in Turbulence," *Transition and Turbulence*, edited by R. E. Meyer, Mathematics Research Center, The Univ. of Wisconsin, Wisconsin, Madison, Oct. 1980, pp. 215–242.

[107] Beneddine, S., Sipp, D., Arnault, A., Dandois, J., and Lesshafft, L., "Conditions for Validity of Mean Flow Stability Analysis and Application to the Determination of Coherent Structures in a Turbulent Backward Facing Step Flow," *Journal of Fluid Mechanics*, Vol. 798, July 2016, pp. 485–504.

[108] Illingworth, S. J., Monty, J. P., and Marusic, I., "Estimating Large-Scale Structures in Wall Turbulence Using Linear Models," *Journal of Fluid Mechanics*, Vol. 842, May 2018, pp. 146–162.

[109] Zare, A., Jovanović, M. R., and Georgiou, T. T., "Colour of Turbulence," *Journal of Fluid Mechanics*, Vol. 812, Feb. 2017, pp. 636–680.

[110] Towne, A., Lozano-Duran, A., and Yang, X., "Resolvent-Based Estimation of Space-Time Flow Statistics," arXiv preprint arXiv:1901.07478, 2019.

[111] Chomaz, J. M., "Global Instabilities in Spatially Developing Flows: Non-Normality and Nonlinearity," *Annual Review of Fluid Mechanics*, Vol. 37, Feb. 2005, pp. 357–392.

[112] Bagheri, S., Brandt, L., and Henningson, D. S., "Input-Output Analysis, Model Reduction and Control Design of the Flat-Plate Boundary Layer," *Journal of Fluid Mechanics*, Vol. 620, Feb. 2009, pp. 263–298.

[113] Barbagallo, A., Sipp, D., and Schmid, P. J., "Closed-Loop Control of an Open Cavity Flow Using Reduced-Order Models," *Journal of Fluid Mechanics*, Vol. 641, Dec. 2009, pp. 1–50.

[114] Åkervik, E., Hœpffner, J., Ehrenstein, U., and Henningson, D. S., "Optimal Growth, Model Reduction and Control in a Separated Boundary-Layer Flow Using Global Eigenmodes," *Journal of Fluid Mechanics*, Vol. 579, May 2007, pp. 305–314.

[115] Bagheri, S., Hœpffner, J., Schmid, P. J., and Henningson, D. S., "Input-Output Analysis and Control Design Applied to a Linear Model of Spatially Developing Flows," *Applied Mechanics Reviews*, Vol. 62, No. 2, 2009, Paper 020803.

[116] Fabbiane, N., Simon, B., Fischer, F., Grundmann, S., Bagheri, S., and Henningson, D. S., "On the Role of Adaptivity for Robust Laminar

Flow Control," *Journal of Fluid Mechanics*, Vol. 767, March 2015, p. R1.
[117] Simon, B., Fabbiane, N., Nemitz, T., Bagheri, S., Henningson, D. S., and Grundmann, S., "In-Flight Active Wave Cancelation with Delayed-x-LMS Control Algorithm in a Laminar Boundary Layer," *Experiments in Fluids*, Vol. 57, No. 10, 2016, p. 160.
[118] Hervé, A., Sipp, D., Schmid, P. J., and Samuelides, M., "A Physics-Based Approach to Flow Control Using System Identification," *Journal of Fluid Mechanics*, Vol. 702, July 2012, pp. 26–58.
[119] Iñigo, J. G., Sipp, D., and Schmid, P. J., "Recovery of the Inherent Dynamics of Noise-Driven Amplifier Flows," *Journal of Fluid Mechanics*, Vol. 797, June 2016, pp. 130–145.
[120] Wu, J.-Z., Lu, X.-Y., Denny, A. G., Fan, M., and Wu, J.-M., "Post-Stall Flow Control on an Airfoil by Local Unsteady Forcing," *Journal of Fluid Mechanics*, Vol. 371, Sept. 1998, pp. 21–58.
[121] Gopalakrishnan Meena, M., Taira, K., and Asai, K., "Airfoil-Wake Modification with Gurney Flap at Low Reynolds Number," *AIAA Journal*, Vol. 56, No. 4, 2017, pp. 1348–1359.
[122] LeGresley, P., and Alonso, J., "Airfoil Design Optimization Using Reduced Order Models Based on Proper Orthogonal Decomposition," AIAA Paper 2000-2545, 2000.
[123] Thomareis, N., and Papadakis, G., "Effect of Trailing Edge Shape on the Separated Flow Characteristics Around an Airfoil at Low Reynolds Number: A Numerical Study," *Physics of Fluids*, Vol. 29, No. 1, 2017, Paper 014101.
[124] Devenport, W. J., Rife, M. C., Liapis, S. I., and Follin, G. J., "The Structure and Development of a Wing-Tip Vortex," *Journal of Fluid Mechanics*, Vol. 312, April 1996, pp. 67–106.
[125] Del Pino, C., Lopez-Alonso, J. M., Parras, L., and Fernandez-Feria, R., "Dynamics of the Wing-Tip Vortex in the Near Field of a NACA 0012 Aerofoil," *Aeronautical Journal*, Vol. 115, No. 1166, 2011, pp. 229–239.
[126] Edstrand, A. M., Davis, T. B., Schmid, P. J., Taira, K., and Cattafesta, L. N., "On the Mechanism of Trailing Vortex Wandering," *Journal of Fluid Mechanics*, Vol. 801, Aug. 2016, p. R1.
[127] Edstrand, A. M., Sun, Y., Schmid, P. J., Taira, K., and Cattafesta, L. N., "Active Attenuation of a Trailing Vortex Inspired by a Parabolized Stability Analysis," *Journal of Fluid Mechanics*, Vol. 855, Nov. 2018, p. R2.
[128] Tam, C. K. W., and Ju, H., "Aerofoil Tones at Moderate Reynolds Number," *Journal of Fluid Mechanics*, Vol. 690, Jan. 2012, pp. 536–570.
[129] Fosas de Pando, M., Schmid, P. J., and Sipp, D., "A Global Analysis of Tonal Noise in Flows Around Aerofoils," *Journal of Fluid Mechanics*, Vol. 754, Sept. 2014, pp. 5–38.
[130] Ribeiro, J. H. M., and Wolf, W. R., "Identification of Coherent Structures in the Flow Past a NACA0012 Airfoil Via Proper Orthogonal Decomposition," *Physics of Fluids*, Vol. 29, No. 8, 2017, Paper 085104.
[131] Liepmann, H. W., "Extension of the Statistical Approach to Buffeting and Gust Response of Wings of Finite Span," *Journal of the Aeronautical Sciences*, Vol. 22, No. 3, 1955, pp. 197–200.
[132] Roos, F. W., "Some Features of the Unsteady Pressure Field in Transonic Airfoil Buffeting," *Journal of Aircraft*, Vol. 17, No. 11, 1980, pp. 781–788.
[133] Raveh, D. E., "Numerical Study of an Oscillating Airfoil in Transonic Buffeting Flows," *AIAA Journal*, Vol. 47, No. 3, 2009, pp. 505–515.
[134] Crouch, J. D., Garbaruk, A., Magidov, D., and Travin, A., "Origin of Transonic Buffet on Aerofoils," *Journal of Fluid Mechanics*, Vol. 628, June 2009, pp. 357–369.
[135] Mohan, A. T., and Gaitonde, D. V., "Analysis of Airfoil Stall Control Using Dynamic Mode Decomposition," *Journal of Aircraft*, Vol. 54, No. 4, 2017, pp. 1508–1520.
[136] Ricciardi, T. R., Ribeiro, J. H. M., and Wolf, W. R., "Analysis of Coherent Structures in Large-Eddy Simulations of a NACA0012 Airfoil," AIAA Paper 2019-0320, 2019.
[137] Freund, J. B., and Colonius, T., "Turbulence and Sound-Field POD Analysis of a Turbulent Jet," *International Journal of Aeroacoustics*, Vol. 8, No. 4, 2009, pp. 337–354.
[138] Theofilis, V., "Global Instabilities and Control of Nonparallel Flows," AIAA Paper 2002-3279, 2002.
[139] Zhang, W., and Samtaney, R., "BiGlobal Linear Stability Analysis on Low-Re Flow Past an Airfoil at High Angle of Attack," *Physics of Fluids*, Vol. 28, No. 4, 2016, Paper 044105.
[140] He, W., Gioria, R. S., Pérez, J. M., and Theofilis, V., "Linear Instability of Low Reynolds Number Massively Separated Flow Around Three NACA Airfoils," *Journal of Fluid Mechanics*, Vol. 811, Jan. 2017, pp. 701–741.
[141] Carr, L. W., "Progress in Analysis and Prediction of Dynamic Stall," *Journal of Aircraft*, Vol. 25, No. 1, 1988, pp. 6–17.
[142] Garmann, D. J., and Visbal, M. R., "Numerical Investigation of Transitional Flow over a Rapidly Pitching Plate," *Physics of Fluids*, Vol. 23, No. 9, 2011, Paper 094106.
[143] Jantzen, R. T., Taira, K., Granlund, K., and Ol, M. V., "Vortex Dynamics Around Pitching Plates," *Physics of Fluids*, Vol. 26, No. 5, 2014, Paper 053696.
[144] Benton, S. I., and Visbal, M. R., "The Onset of Dynamic Stall at a High, Transitional Reynolds Number," *Journal of Fluid Mechanics*, Vol. 861, Feb. 2019, pp. 860–885.
[145] Greenblatt, D., and Wygnanski, I. J., "The Control of Flow Separation by Periodic Excitation," *Progress in Aerospace Sciences*, Vol. 36, No. 7, 2000, pp. 487–545.
[146] Amitay, M., and Glezer, A., "Role of Actuation Frequency in Controlled Flow Reattachment over a Stalled Airfoil," *AIAA Journal*, Vol. 40, No. 2, 2002, pp. 209–216.
[147] Munday, P. M., and Taira, K., "Effects of Wall-Normal and Angular Momentum Injections in Airfoil Separation Control," *AIAA Journal*, Vol. 56, No. 5, 2018, pp. 1830–1842.
[148] Jovanović, M. R., "Modeling, Analysis, and Control of Spatially Distributed Systems," Ph.D. Thesis, Dept. of Mechanical Engineering, Univ. of California, Santa Barbara, Santa Barbara, CA, 2004.
[149] Crouch, J., "Airplane Trailing Vortices and Their Control," *Comptes Rendus Physique*, Vol. 6, Nos. 4–5, 2005, pp. 487–499.
[150] Bailey, S. C. C., and Tavoularis, S., "Measurements of the Velocity Field of a Wing-Tip Vortex, Wandering in Grid Turbulence," *Journal of Fluid Mechanics*, Vol. 601, April 2008, pp. 281–315.
[151] Margaris, P., and Gursul, I., "Vortex Topology of Wing Tip Blowing," *Aerospace Science and Technology*, Vol. 14, No. 3, 2010, pp. 143–160.
[152] Edstrand, A., and Cattafesta, L. N., "Topology of a Trailing Vortex Flow Field with Steady Circulation Control Blowing," AIAA Paper 2015-1706, 2015.
[153] He, W., Tendero, J. A., Paredes, P., and Theofilis, V., "Linear Instability in the Wake of an Elliptic Wing," *Theoretical and Computational Fluid Dynamics*, Vol. 31, Nos. 5–6, 2017, pp. 483–504.
[154] Lawson, S. J., and Barakos, G. N., "Review of Numerical Simulations for High-Speed, Turbulent Cavity Flows," *Progress in Aerospace Sciences*, Vol. 47, No. 3, 2011, pp. 186–216.
[155] Rossiter, J. E., "Wind-Tunnel Experiments on the Flow over Rectangular Cavities at Subsonic and Transonic Speeds," Aeronautical Research Council, TR 3438, 1964.
[156] Ahuja, K. K., and Mendoza, J., "Effects of Cavity Dimensions, Boundary Layer and Temperature on Cavity Noise with Emphasis on Benchmark Data to Validate Computational Aeroacoustic Codes," NASA TR 4653, Hampton, VA, 1995.
[157] Murray, N., Sällström, E., and Ukeiley, L., "Properties of Subsonic Open Cavity Flow Fields," *Physics of Fluids*, Vol. 21, No. 9, 2009, p. 1661.
[158] Beresh, S. J., Wagner, J. L., and Casper, K. M., "Compressibility Effects in the Shear Layer over a Rectangular Cavity," *Journal of Fluid Mechanics*, Vol. 808, Oct. 2016, pp. 116–152.
[159] Brès, G. A., and Colonius, T., "Three-Dimensional Instabilities in Compressible Flow over Open Cavities," *Journal of Fluid Mechanics*, Vol. 599, March 2008, pp. 309–339.
[160] Yamouni, S., Sipp, D., and Jacquin, L., "Interaction Between Feedback Aeroacoustic and Acoustic Resonance Mechanisms in a Cavity Flow: A Global Stability Analysis," *Journal of Fluid Mechanics*, Vol. 717, Feb. 2013, pp. 134–165.
[161] Vicente, J., Basley, J., Meseguer-Garrido, F., Soria, J., and Theofilis, V., "Three-Dimensional Instabilities over a Rectangular Open Cavity: From Linear Stability Analysis to Experimentation," *Journal of Fluid Mechanics*, Vol. 748, June 2014, pp. 189–220.
[162] Sun, Y., Taira, K., Cattafesta, L. N., and Ukeiley, L. S., "Spanwise Effects on Instabilities of Compressible Flow over a Long Rectangular Cavity," *Theoretical and Computational Fluid Dynamics*, Vol. 31, Nos. 5–6, 2017, pp. 555–565.
[163] Sun, Y., Taira, K., Cattafesta, L. N., and Ukeiley, L. S., "Biglobal Stability Analysis of Compressible Open Cavity Flow," *Journal of Fluid Mechanics*, Vol. 826, Sept. 2017, pp. 270–301.
[164] Liu, Q., Sun, Y., Cattafesta, L. N., Ukeiley, L. S., and Taira, K., "Resolvent Analysis of Compressible Flows over a Long Rectangular Cavity," AIAA Paper 2018-0588, 2018.
[165] Qadri, U. A., and Schmid, P. J., "Frequency Selection Mechanisms in the Flow of a Laminar Boundary Layer over a Shallow Cavity," *Physical Review Fluids*, Vol. 2, No. 1, 2017, Paper 013902.
[166] Crook, S. D., Lau, T. C. W., and Kelso, R. M., "Three-Dimensional Flow Within Shallow, Narrow Cavities," *Journal of Fluid Mechanics*, Vol. 735, Nov. 2013, pp. 587–612.

[167] Ohmichi, Y., and Suzuki, K., "Flow Structures and Heating Augmentation Around Finite-Width Cavity in Hypersonic Flow," *AIAA Journal*, Vol. 52, No. 8, 2014, pp. 1624–1631.

[168] Sun, Y., Liu, Q., Cattafesta, L. N., Ukeiley, L. S., and Taira, K., "Effects of Sidewalls and Leading-Edge Blowing on Flows over Long Rectangular Cavities," *AIAA Journal*, Vol. 57, No. 1, 2019, pp. 106–119.

[169] Liu, Q., Gómez, F., and Theofilis, V., "Linear Instability Analysis of Low-Re Incompressible Flow over a Long Rectangular Finite-Span Open Cavity," *Journal of Fluid Mechanics*, Vol. 799, July 2016, p. R2.

[170] Shaw, L., and Northcraft, S., "Close Loop Active Control for Cavity Acoustics," AIAA Paper 1999-1902, 1999.

[171] Ukeiley, L. S., Ponton, M. K., Seiner, J. M., and Jansen, B., "Suppression of Pressure Loads in Cavity Flows," *AIAA Journal*, Vol. 42, No. 1, 2004, pp. 77–79.

[172] Dudley, J. G., and Ukeiley, L., "Passively Controlled Supersonic Cavity Flow Using a Spanwise Cylinder," *Experiments in Fluids*, Vol. 55, No. 9, 2014, p. 1810.

[173] Ukeiley, L., Sheehan, M., Coiffet, F., Alvi, F., Arunajatesan, S., and Jansen, B., "Control of Pressure Loads in Geometrically Complex Cavities," *Journal of Aircraft*, Vol. 44, No. 9, 2008, pp. 2118–2128.

[174] Takahashi, H., Liu, F., Palaviccini, M., Oyarzun, M., Griffin, J., Ukeiley, L., and Cattafesta, L., "Experimental Study of Adaptive Control of High-Speed Flow-Induced Cavity Oscillations," *Journal of Fluid Science and Technology*, Vol. 6, No. 5, 2011, pp. 701–716.

[175] Zhang, Y., Sun, Y., Arora, N., Cattafesta, L. N., Taira, K., and Ukeiley, L. S., "Suppression of Cavity Flow Oscillations via Three-Dimensional Steady Blowing," *AIAA Journal*, Vol. 57, No. 1, 2019, pp. 90–105.

[176] Hunt, J. C. R., Wray, A. A., and Moin, P., "Eddies, Streams, and Convergence Zones in Turbulent Flows," *Proceedings of the 1988 Summer Program*, Center for Turbulence Research, Stanford, CA, 1988, pp. 193–208.

[177] George, B., Ukeiley, L., Cattafesta, L., and Taira, K., "Control of Three-Dimensional Cavity Flow Using Leading-Edge Slot Blowing," AIAA Paper 2015-1059, 2015.

[178] Lusk, W. T., Cattafesta, L. N., and Ukeiley, L. S., "Leading Edge Slot Blowing on an Open Cavity in Supersonic Flow," *Experiments in Fluids*, Vol. 53, No. 1, 2012, pp. 187–199.

[179] Barbagallo, A., Sipp, D., and Schmid, P. J., "Closed-Loop Control of an Open Cavity Flow Using Reduced-Order Models," *Journal of Fluid Mechanics*, Vol. 641, Dec. 2009, pp. 1–50.

[180] Ricciardi, T. R., Wolf, W. R., Kreitzman, J., Moffitt, N. J., and Bent, P., "An Assessment of High-Fidelity Flow Simulation Methodologies for Noise Prediction of Realistic Landing Gear Configurations," AIAA Paper 2019-0003, 2019.

[181] Sieber, M., Paschereit, C. O., and Oberleithner, K., "Spectral Proper Orthogonal Decomposition," *Journal of Fluid Mechanics*, Vol. 792, April 2016, pp. 798–828.

[182] Roweis, S. T., and Saul, L. K., "Nonlinear Dimensionality Reduction by Locally Linear Embedding," *Science*, Vol. 290, No. 5500, 2000, pp. 2323–2326.

[183] Ehlert, A., Nayeri, C. N., Morzynski, M., and Noack, B. R., "Locally Linear Embedding for Transient Cylinder Wakes," arXiv preprint arXiv:1906.07822, 2019.

[184] Amsallem, D., and Farhat, C., "Interpolation Method for Adapting Reduced-Order Models and Application to Aeroelasticity," *AIAA Journal*, Vol. 46, No. 7, 2008, pp. 1803–1813.

[185] Loiseau, J.-C., Brunton, S. L., and Noack, B. R., "From the POD-Galerkin Method to Sparse Manifold Models," *Handbook of Model-Order Reduction, Volume 2: Applications*, edited by P. Benner, de Gruyter, Berlin, 2019, pp. 1–47.

[186] Milano, M., and Koumoutsakos, P., "Neural Network Modeling for Near Wall Turbulent Flow," *Journal of Computational Physics*, Vol. 182, No. 1, 2002, pp. 1–26.

[187] Murata, T., Fukami, K., and Fukagata, K., "Nonlinear Mode Decomposition with Machine Learning for Fluid Dynamics," arXiv preprint arXiv:1906.04029, 2019.

[188] Hornik, K., Stinchcombe, M., and White, H., "Multilayer Feedforward Networks Are Universal Approximators," *Neural Networks*, Vol. 2, No. 5, 1989, pp. 359–366.

[189] Krizhevsky, A., Sutskever, I., and Hinton, G. E., "ImageNet Classification with Deep Convolutional Neural Networks," *Advances in Neural Information Processing Systems*, San Diego, CA, 2012, pp. 1097–1105.

[190] LeCun, Y., Bengio, Y., and Hinton, G., "Deep Learning," *Nature*, Vol. 521, No. 7553, 2015, pp. 436–444.

[191] Goodfellow, I., Bengio, Y., and Courville, A., *Deep Learning*, MIT Press, Cambridge, MA, 2016.

[192] Wehmeyer, C., and Noé, F., "Time-Lagged Autoencoders: Deep Learning of Slow Collective Variables for Molecular Kinetics," *Journal of Chemical Physics*, Vol. 148, No. 24, 2018, Paper 241703.

[193] Mardt, A., Pasquali, L., Wu, H., and Noé, F., "VAMPnets: Deep Learning of Molecular Kinetics," *Nature Communications*, Vol. 9, No. 5, 2018.

[194] Takeishi, N., Kawahara, Y., and Yairi, T., "Learning Koopman Invariant Subspaces for Dynamic Mode Decomposition," *Advances in Neural Information Processing Systems*, San Diego, CA, 2017, pp. 1130–1140.

[195] Yeung, E., Kundu, S., and Hodas, N., "Learning Deep Neural Network Representations for Koopman Operators of Nonlinear Dynamical Systems," arXiv preprint arXiv:1708.06850, 2017.

[196] Otto, S. E., and Rowley, C. W., "Linearly Recurrent Autoencoder Networks for Learning Dynamics," *SIAM Journal on Applied Dynamical Systems*, Vol. 18, No. 1, 2019, pp. 558–593.

[197] Lusch, B., Kutz, J. N., and Brunton, S. L., "Deep Learning for Universal Linear Embeddings of Nonlinear Dynamics," *Nature Communications*, Vol. 9, No. 1, 2018, p. 4950.

[198] Mezić, I., "Spectral Properties of Dynamical Systems, Model Reduction and Decompositions," *Nonlinear Dynamics*, Vol. 41, Nos. 1–3, 2005, pp. 309–325.

[199] Brunton, S. L., Brunton, B. W., Proctor, J. L., and Kutz, J. N., "Koopman Observable Subspaces and Finite Linear Representations of Nonlinear Dynamical Systems for Control," *PLoS ONE*, Vol. 11, No. 2, 2016, Paper e0150171.

[200] Brunton, S. L., and Kutz, J. N., *Data-Driven Science and Engineering: Machine Learning, Dynamical Systems, and Control*, Cambridge Univ. Press, Cambridge, 2019.

[201] Manohar, K., Brunton, B. W., Kutz, J. N., and Brunton, S. L., "Data-Driven Sparse Sensor Placement," *IEEE Control Systems Magazine*, Vol. 38, No. 3, 2018, pp. 63–86.

[202] Mohren, T. L., Daniel, T. L., Brunton, S. L., and Brunton, B. W., "Neural-Inspired Sensors Enable Sparse, Efficient Classification of Spatiotemporal Data," *Proceedings of the National Academy of Sciences*, Vol. 115, No. 42, 2018, pp. 10564–10569.

[203] Halko, N., Martinsson, P.-G., and Tropp, J. A., "Finding Structure with Randomness: Probabilistic Algorithms for Constructing Approximate Matrix Decompositions," *SIAM Review*, Vol. 53, No. 2, 2011, pp. 217–288.

[204] Bourguignon, J.-L., Tropp, J., Sharma, A., and McKeon, B., "Compact Representation of Wall-Bounded Turbulence Using Compressive Sampling," *Physics of Fluids*, Vol. 26, No. 1, 2014, Paper 015109.

[205] Bai, Z., Wimalajeewa, T., Berger, Z., Wang, G., Glauser, M., and Varshney, P. K., "Low-Dimensional Approach for Reconstruction of Airfoil Data via Compressive Sensing," *AIAA Journal*, Vol. 53, No. 4, 2014, pp. 920–933.

[206] Bright, I., Lin, G., and Kutz, J. N., "Compressive Sensing and Machine Learning Strategies for Characterizing the Flow Around a Cylinder with Limited Pressure Measurements," *Physics of Fluids*, Vol. 25, No. 12, 2013, Paper 127102.

[207] Kramer, B., Grover, P., Boufounos, P., Benosman, M., and Nabi, S., "Sparse Sensing and DMD Based Identification of Flow Regimes and Bifurcations in Complex Flows," *SIAM Journal on Applied Dynamical Systems*, Vol. 16, No. 2, 2017, pp. 1164–1196.

[208] Brunton, B. W., Brunton, S. L., Proctor, J. L., and Kutz, J. N., "Sparse Sensor Placement Optimization for Classification," *SIAM Journal on Applied Mathematics*, Vol. 76, No. 5, 2016, pp. 2099–2122.

[209] Mahoney, M. W., "Randomized Algorithms for Matrices and Data," *Foundations and Trends in Machine Learning*, Vol. 3, No. 2, 2011, pp. 123–224.

[210] Rokhlin, V., Szlam, A., and Tygert, M., "A Randomized Algorithm for Principal Component Analysis," *SIAM Journal on Matrix Analysis and Applications*, Vol. 31, No. 3, 2009, pp. 1100–1124.

[211] Halko, N., Martinsson, P.-G., Shkolnisky, Y., and Tygert, M., "An Algorithm for the Principal Component Analysis of Large Data Sets," *SIAM Journal on Scientific Computing*, Vol. 33, No. 5, 2011, pp. 2580–2594.

[212] Bistrian, D., and Navon, I., "Randomized Dynamic Mode Decomposition for Nonintrusive Reduced Order Modelling," *International Journal for Numerical Methods in Engineering*, Vol. 112, No. 1, 2017, pp. 3–0.

[213] Erichson, N. B., Mathelin, L., Kutz, J. N., and Brunton, S. L., "Randomized Dynamic Mode Decomposition," arXiv preprint arXiv:1702.02912, 2017.

[214] Ribeiro, J. H. M., Yeh, C.-A., and Taira, K., "Randomized Resolvent Analysis," arXiv preprint arXiv:1902.01458, 2019.

[215] Benner, P., Gugercin, S., and Willcox, K., "A Survey of Projection-Based Model Reduction Methods for Parametric Dynamical Systems," *SIAM Review*, Vol. 57, No. 4, 2015, pp. 483–531.

[216] Lui, H. F. S., and Wolf, W. R., "Construction of Reduced-Order Models for Fluid Flows Using Deep Feedforward Neural Networks," *Journal of Fluid Mechanics*, Vol. 872, Aug. 2019, pp. 963–994.
[217] Glaz, B., Liu, L., and Friedmann, P. P., "Reduced-Order Nonlinear Unsteady Aerodynamic Modeling Using a Surrogate-Based Recurrence Framework," *AIAA Journal*, Vol. 48, No. 10, 2010, pp. 2418–2429.
[218] Williams, M. O., Rowley, C. W., and Kevrekidis, I. G., "A Kernel Approach to Data-Driven Koopman Spectral Analysis," *Journal of Computational Dynamics*, Vol. 2, No. 2, 2015, pp. 247–265.
[219] Williams, M. O., Kevrekidis, I. G., and Rowley, C. W., "A Data-Driven Approximation of the Koopman Operator: Extending Dynamic Mode Decomposition," *Journal of Nonlinear Science*, Vol. 25, No. 6, 2015, pp. 1307–1346.
[220] Semeraro, O., Lusseyran, F., Pastur, L., and Jordan, P., "Qualitative Dynamics of Wave Packets in Turbulent Jets," *Physical Review Fluids*, Vol. 2, No. 9, 2017, Paper 094605.
[221] Wan, Z. Y., Vlachas, P., Koumoutsakos, P., and Sapsis, T., "Data-Assisted Reduced-Order Modeling of Extreme Events in Complex Dynamical Systems," *PloS One*, Vol. 13, No. 5, 2018, pp. 1–22.
[222] Vlachas, P. R., Byeon, W., Wan, Z. Y., Sapsis, T. P., and Koumoutsakos, P., "Data-Driven Forecasting of High-Dimensional Chaotic Systems with Long Short-Term Memory Networks," *Proceedings of the Royal Society A: Mathematical, Physical and Engineering Sciences*, Vol. 474, No. 2213, 2018.
[223] Raissi, M., and Karniadakis, G. E., "Hidden Physics Models: Machine Learning of Nonlinear Partial Differential Equations," *Journal of Computational Physics*, Vol. 357, March 2018, pp. 125–141.
[224] Raissi, M., Perdikaris, P., and Karniadakis, G., "Physics-Informed Neural Networks: A Deep Learning Framework for Solving Forward and Inverse Problems Involving Nonlinear Partial Differential Equations," *Journal of Computational Physics*, Vol. 378, Feb. 2019, pp. 686–707.
[225] Mohebujjaman, M., Rebholz, L., and Iliescu, T., "Physically-Constrained Data-Driven, Filtered Reduced Order Modeling of Fluid Flows," arXiv preprint arXiv:1806.00350, 2018.
[226] Ling, J., and Templeton, J., "Evaluation of Machine Learning Algorithms for Prediction of Regions of High Reynolds Averaged Navier Stokes Uncertainty," *Physics of Fluids*, Vol. 27, No. 8, 2015, Paper 085103.
[227] Parish, E. J., and Duraisamy, K., "A Paradigm for Data-Driven Predictive Modeling Using Field Inversion and Machine Learning," *Journal of Computational Physics*, Vol. 305, Jan. 2016, pp. 758–774.
[228] Ling, J., Kurzawski, A., and Templeton, J., "Reynolds Averaged Turbulence Modelling Using Deep Neural Networks with Embedded Invariance," *Journal of Fluid Mechanics*, Vol. 807, Nov. 2016, pp. 155–166.
[229] Xiao, H., Wu, J.-L., Wang, J.-X., Sun, R., and Roy, C., "Quantifying and Reducing Model-Form Uncertainties in Reynolds-Averaged Navier–Stokes Simulations: A Data-Driven, Physics-Informed Bayesian Approach," *Journal of Computational Physics*, Vol. 324, Nov. 2016, pp. 115–136.
[230] Singh, A. P., Medida, S., and Duraisamy, K., "Machine-Learning-Augmented Predictive Modeling of Turbulent Separated Flows over Airfoils," *AIAA Journal*, Vol. 55, No. 7, 2017, pp. 2215–2227.
[231] Wang, J.-X., Wu, J.-L., and Xiao, H., "Physics-Informed Machine Learning Approach for Reconstructing Reynolds Stress Modeling Discrepancies Based on DNS Data," *Physical Review Fluids*, Vol. 2, No. 3, 2017, Paper 034603.
[232] Maulik, R., San, O., Rasheed, A., and Vedula, P., "Subgrid Modelling for Two-Dimensional Turbulence Using Neural Networks," *Journal of Fluid Mechanics*, Vol. 858, Jan. 2019, pp. 122–144.
[233] Duraisamy, K., Iaccarino, G., and Xiao, H., "Turbulence Modeling in the Age of Data," *Annual Review of Fluid Mechanics*, Vol. 51, No. 1, 2019, pp. 357–377.
[234] Rudy, S. H., Brunton, S. L., Proctor, J. L., and Kutz, J. N., "Data-Driven Discovery of Partial Differential Equations," *Science Advances*, Vol. 3, No. 4, 2017, Paper e1602614.
[235] Hemati, M. S., Dawson, S. T. M., and Rowley, C. W., "Parameter-Varying Aerodynamics Models for Aggressive Pitching-Response Prediction," *AIAA Journal*, Vol. 55, No. 3, 2017, pp. 693–701.
[236] Newman, M., Barabási, A.-L., and Watts, D. J., *The Structure and Dynamics of Networks*, Princeton Univ. Press, Princeton, NJ, 2006.
[237] Newman, M. E. J., *Networks: An Introduction*, Oxford Univ. Press, Oxford, 2010.
[238] Kaiser, E., Noack, B. R., Cordier, L., Spohn, A., Segond, M., Abel, M., Daviller, G., and Niven, R. K., "Cluster-Based Reduced-Order Modelling of a Mixing Layer," *Journal of Fluid Mechanics*, Vol. 754, Sept. 2014, pp. 365–414.
[239] Nair, A. G., Yeh, C. A., Kaiser, E., Noack, B. R., Brunton, S. L., and Taira, K., "Cluster-Based Feedback Control of Turbulent Post-Stall Separated Flows," *Journal of Fluid Mechanics*, Vol. 875, Sept. 2019, pp. 345–375.
[240] Nair, A. G., and Taira, K., "Network-Theoretic Approach to Sparsified Discrete Vortex Dynamics," *Journal of Fluid Mechanics*, Vol. 768, April 2015, pp. 549–571.
[241] Taira, K., Nair, A. G., and Brunton, S. L., "Network Structure of Two-Dimensional Decaying Isotropic Turbulence," *Journal of Fluid Mechanics*, Vol. 795, May 2016, p. R2.
[242] Meena, M. G., Nair, A. G., and Taira, K., "Network Community-Based Model Reduction for Vortical Flows," *Physical Review E*, Vol. 97, No. 6, 2018, Paper 063103.
[243] Proctor, J. L., Brunton, S. L., and Kutz, J. N., "Dynamic Mode Decomposition with Control," *SIAM Journal on Applied Dynamical Systems*, Vol. 15, No. 1, 2016, pp. 142–161.
[244] Williams, M. O., Kevrekidis, I. G., and Rowley, C. W., "A Data-Driven Approximation of the Koopman Operator: Extending Dynamic Mode Decomposition," *Journal of Nonlinear Science*, Vol. 25, No. 6, 2015, pp. 1307–1346.
[245] Hemati, M. S., Williams, M. O., and Rowley, C. W., "Dynamic Mode Decomposition for Large and Streaming Datasets," *Physics of Fluids*, Vol. 26, No. 11, 2014, Paper 111701.
[246] Zhang, H., Rowley, C. W., Deem, E. A., and Cattafesta, L. N., "Online Dynamic Mode Decomposition for Time-Varying Systems," arXiv preprint, arXiv:1707.02876, 2017.
[247] Korda, M., and Mezić, I., "Linear Predictors for Nonlinear Dynamical Systems: Koopman Operator Meets Model Predictive Control," *Automatica*, Vol. 93, July 2018, pp. 149–160.
[248] Kaiser, E., Kutz, J. N., and Brunton, S. L., "Sparse Identification of Nonlinear Dynamics for Model Predictive Control in the Low-Data Limit," *Proceedings of the Royal Society A: Mathematical, Physical and Engineering Sciences*, Vol. 474, No. 2219, 2018, Paper 20180335.
[249] Arbabi, H., Korda, M., and Mezic, I., "A Data-Driven Koopman Model Predictive Control Framework for Nonlinear Flows," arXiv preprint arXiv:1804.05291, 2018.
[250] Deem, E., Cattafesta, L., Yao, H., Hemati, M., Zhang, H., and Rowley, C., "Experimental Implementation of Modal Approaches for Autonomous Reattachment of Separated Flows," AIAA Paper 2018-1052, 2018.
[251] Wang, Z., "Reduced-Order Modeling of Complex Engineering and Geophysical Flows: Analysis and Computations," Ph.D. Thesis, Virginia Polytechnic Inst. and State Univ., Blacksburg, VA, 2012.
[252] Kalashnikova, I., Arunajatesan, S., Barone, M. F., van Bloemen Waanders, B. G., and Fike, J. A., "Reduced Order Modeling for Prediction and Control of Large-Scale Systems," Sandia National Lab., Rept. SAND2014-4693, Albuquerque, NM, May 2014.
[253] Rowley, C. W., Colonius, T., and Murray, R. M., "Model Reduction for Compressible Flows Using POD and Galerkin Projection," *Physica D: Nonlinear Phenomena*, Vol. 189, Nos. 1–2, 2004, pp. 115–129.
[254] Sirovich, L., "Turbulence and the Dynamics of Coherent Structures: I, II and III," *Quarterly Applied Mathematics*, Vol. 45, No. 3, 1987, pp. 561–590.
[255] Carlberg, K., Bou-Mosleh, C., and Farhat, C., "Efficient Non-Linear Model Reduction via a Least-Squares Petrov–Galerkin Projection and Compressive Tensor Approximations," *International Journal for Numerical Methods in Engineering*, Vol. 86, No. 2, 2011, pp. 155–181.
[256] Ullmann, S., and Lang, J., "A POD-Galerkin Reduced Model with Updated Coefficients for Smagorinsky LES," *Proceedings of the V European Conference on Computational Fluid Dynamics, ECCOMAS CFD*, edited by J. C. F. Pereira, and A. Sequeira, ECCOMAS, Barcelona, 2010.
[257] Wang, Z., Akhtar, I., Borggaard, J., and Iliescu, T., "Two-Level Discretizations of Nonlinear Closure Models for Proper Orthogonal Decomposition," *Journal of Computational Physics*, Vol. 230, No. 1, 2011, pp. 126–146.
[258] Noack, B., Papas, P., and Monkewitz, P., "Low-Dimensional Galerkin Model of a Laminar Shear-Layer," École Polytechnique Fédérale de Lausanne Rept. 2002-01, Lausanne, Switzerland, 2002.
[259] San, O., and Iliescu, T., "A Stabilized Proper Orthogonal Decomposition Reduced-Order Model for Large Scale Quasigeostrophic Ocean Circulation," *Advances in Computational Mathematics*, Vol. 41, No. 1, 2015, pp. 1289–1319.
[260] Bergmann, M., Bruneaua, C., and Iollo, A., "Enablers for Robust POD Models," *Journal of Computational Physics*, Vol. 228, No. 1, 2009, pp. 516–538.
[261] Chorin, A. J., and Hald, O. H., *Stochastic Tools for Mathematics and Science*, Springer, New York, 2013.

[262] Stinis, P., "Mori–Zwanzig Reduced Models for Uncertainty Quantification I: Parametric Uncertainty," arXiv preprint arXiv:1211.4285, 2012.
[263] Parish, E. J., and Duraisamy, K., "Non-Markovian Closure Models for Large Eddy Simulations Using the Mori–Zwanzig Formalism," *Physical Review Fluids*, Vol. 2, No. 1, 2017, Paper 014604.
[264] Parish, E. J., and Duraisamy, K., "A Dynamic Subgrid Scale Model for Large Eddy Simulations Based on the Mori–Zwanzig Formalism," *Journal of Computational Physics*, Vol. 349, Nov. 2017, pp. 154–175.
[265] Gouasmi, A., Parish, E. J., and Duraisamy, K., "A Priori Estimation of Memory Effects in Reduced-Order Models of Nonlinear Systems Using the Mori–Zwanzig Formalism," *Proceedings of the Royal Society A: Mathematical, Physical and Engineering Sciences*, Vol. 473, No. 2205, 2017, Paper 20170385.
[266] Parish, E. J., and Duraisamy, K., "A Unified Framework for Multiscale Modeling Using Mori–Zwanzig and the Variational Multiscale Method," arXiv:1712.09669, 2018.
[267] Parish, E. J., Christopher, W., and Duraisamy, K., "The Adjoint Petrov-Galerkin Method for Non-Linear Model Reduction," arXiv preprint arXiv:1810.03455, 2018.
[268] Everson, R., and Sirovich, L., "Karhunen–Loève Procedure for Gappy Data," *Journal of the Optical Society of America A*, Vol. 12, No. 8, 1995, pp. 1657–1664.
[269] Willcox, K., "Unsteady Flow Sensing and Estimation via the Gappy Proper Orthogonal Decomposition," *Computers and Fluids*, Vol. 35, No. 2, 2006, pp. 208–226.
[270] Barrault, M., Maday, Y., Nguyen, N. C., and Patera, A. T., "An 'Empirical Interpolation' Method: Application to Efficient Reduced-Basis Discretization of Partial Differential Equations," *Comptes Rendus Mathematique*, Vol. 339, No. 9, 2004, pp. 667–672.
[271] Chaturantabut, S., and Sorensen, D. C., "Nonlinear Model Reduction via Discrete Empirical Interpolation," *SIAM Journal on Scientific Computing*, Vol. 32, No. 5, 2010, pp. 2737–2764.
[272] Chaturantabut, S., and Sorensen, D. C., "A State Space Error Estimate for POD-DEIM Nonlinear Model Reduction," *SIAM Journal on Numerical Analysis*, Vol. 50, No. 1, 2012, pp. 46–63.
[273] Peherstorfer, B., Butnaru, D., Willcox, K., and Bungartz, H.-J., "Localized Discrete Empirical Interpolation Method," *SIAM Journal on Scientific Computing*, Vol. 36, No. 1, 2014, pp. A168–A192.
[274] Avellaneda, M., and Majda, A. J., "Mathematical Models with Exact Renormalization for Turbulent Transport," *Communications in Mathematical Physics*, Vol. 131, No. 2, 1990, pp. 381–429.
[275] Amsallem, D., Zahr, M. J., and Farhat, C., "Nonlinear Model Order Reduction Based on Local Reduced-Order Bases," *International Journal for Numerical Methods in Engineering*, Vol. 92, No. 10, 2012, pp. 891–916.
[276] Carlberg, K., Farhat, C., Cortial, J., and Amsallem, D., "The GNAT Method for Nonlinear Model Reduction: Effective Implementation and Application to Computational Fluid Dynamics and Turbulent Flows," *Journal of Computational Physics*, Vol. 242, June 2013, pp. 623–647.

P. Givi
Associate Editor